Remote Sensing of Environment 275 (2022) 112964

Contents lists available at ScienceDirect

Remote Sensing of Environment

journal homepage: www.elsevier.com/locate/rse

Forest aboveground biomass in the southwestern United States from a MISR multi-angle index, 2000–2015

Mark Chopping [a,*], Zhuosen Wang [b,f], Crystal Schaaf [c], Michael A. Bull [d], Rocio R. Duchesne [e]

[a] Department of Earth and Environmental Studies, Montclair State University, Montclair, NJ 07043, United States
[b] Earth System Science Interdisciplinary Center, University of Maryland College Park, College Park, MD 20740, United States
[c] University of Massachusetts Boston, School for the Environment, Boston, MA 02125, United States
[d] NASA Jet Propulsion Laboratory, Pasadena, CA 91109, United States
[e] Department of Geography, Geology, and Environmental Science, University of Wisconsin-Whitewater, Whitewater, WI 51390, United States
[f] Terrestrial Information Systems Laboratory, NASA Goddard Space Flight Center, Greenbelt, MD 20771, United States

ARTICLE INFO

Editor: Jing M. Chen

ABSTRACT

Multi-angle surface reflectance data from the NASA Jet Propulsion Laboratory Multi-angle Imaging SpectroRadiometer (MISR) were used to map aboveground biomass density (AGB, Mg ha^{-1}) in the forests of the southwestern United States inter-annually from 2000 to 2015. The approach uses a multi-angle index that has a $\log_e$ relationship with AGB estimates in the National Biomass and Carbon Dataset 2000 (NBCD 2000). MISR Level 1B2 Terrain radiance data from May 15–June 15 of each year were converted to mapped surface bidirectional reflectance factors (BRFs) and leveraged to adjust the kernel weights of the RossThin-LiSparse-Reciprocal Bidirectional Reflectance Distribution Function (BRDF) model. The kernel weights with the lowest model-fitting RMSE were selected as the least likely to be cloud-contaminated and were used to generate synthetic MISR datasets. An optimal index calculated using BRFs modeled in the solar principal plane was found with respect to NBCD 2000 estimates for 19 sites near Mt. Lindsey, Colorado. These relationships were found in areas with AGB ranging from 20 to 190 Mg ha^{-1}, with the model yielding $R^2 = 0.91$ (RMSE: 15.4 Mg ha^{-1}). With spectral-nadir metrics, the R^2 values obtained were 0.07, 0.32, and 0.37 for NIR band BRFs, NDVI, and red band BRFs, respectively. For regional application, a simplified single coefficient model was fitted to the NBCD 2000 data, to account for variations in forest type, soils, and topography. The resulting AGB maps were consistent with estimates from up-scaled 2005 ICESat GLAS data and 2013 NASA Carbon Monitoring System airborne lidar-derived estimates for the Rim Fire area in California; and with the 2005 GLAS-based map across the southwestern United States. Trajectories were stable through time and losses from fire and beetle disturbance matched historical data in published sources. MISR estimates were found to reliably capture ABG compared to radar- and lidar-derived estimates across the southwestern United States ($N = 11{,}019{,}944$), with an RMSE of 37.0 Mg ha^{-1} and $R^2 = 0.9$ vs GLAS estimates.

1. Introduction

Regional maps of forest aboveground biomass (AGB) are required for a wide range of applications, including the assessment of the impacts of climate change – for example, losses from insect outbreaks, pathogens, wildfire, and drought; estimating fire fuel loading, growth, management, and the potential for particulate and carbon gas emissions to the atmosphere (Duncanson et al., 2019). Active sensing technologies – lidar and radar – are recognized as the most appropriate technologies for mapping forest AGB (Bergen et al., 2009; Xiao et al., 2019; Zhang et al., 2014). However, their spatial and temporal coverage is limited (Herold et al., 2019). On the other hand, passive instruments capable of acquiring near-nadir spectral reflectance values regularly over large areas do not typically provide AGB, as their data are relatively insensitive to 3-D canopy structure (Wang et al., 2016). This study explores an innovative use of a multi-angle passive remote sensing technology that is sensitive to forest 3-D structure and provides an annual record from 2000 onwards. The additional source of information provides a means to more fully investigate the development of forests in this region over a period of accelerating change.

* Corresponding author.
E-mail address: choppingm@mail.montclair.edu (M. Chopping).

https://doi.org/10.1016/j.rse.2022.112964
Received 24 May 2021; Received in revised form 17 January 2022; Accepted 18 February 2022
Available online 8 April 2022

Lidar and radar remote sensing technologies have been used to map forest AGB for many years. Airborne lidar surveys (ALS) provide limited spatial coverage and temporal sampling but have been extemely useful in demonstrating the technology and for focused sub-regional studies (e.g., NASA's Land, Vegetation, and Ice Sensor (LVIS); Chopping et al., 2012), but for larger areas, space-based missions are imperative. The first major effort used Shuttle Radar Topography Mission data to produce the National Biomass and Carbon Dataset 2000 – NBCD 2000, a year 2000 forest AGB map covering the conterminous U.S. – for the North American Carbon Program (Kellndorfer et al., 2013). The NASA Geoscience Laser Altimeter System (GLAS) launched on ICESat in 2003 provides a 6-year record, with ~65 m footprint lidar waveform data sampled at ~200 m intervals. This has been found to be very useful for mapping forest AGB (Lefsky et al., 2005; Saatchi et al., 2011). Both the NBCD 2000 and GLAS-derived AGB datasets are leveraged in this study. The ICESat-2 Advanced Topographic Laser Altimeter System (ATLAS) photon-counting lidar launched in September 2018 has shown it is capable of providing forest canopy height and AGB, even though it is optimized for ice sheet monitoring (Narine et al., 2020). However, NASA's Global Ecosystem Dynamics Investigation (GEDI) is the first dedicated vegetation canopy lidar (VCL) in space. It was launched to the International Space Station in December 2018 and its multiple full waveform lidars provide canopy structure information for eight transects at scales down to 25 m, and forest AGB for all land locations within ±52° latitude (Dubayah et al., 2020). Each GEDI footprint is separated by 60 m along-track and 600 m across-track, with an across-track width of ~4.2 km. In the GEDI AGB density (AGBD) product, relationships between field plot estimates and simulated GEDI Level 2A waveform relative height metrics are captured in a parametric model and used to derive footprint AGBD (Dubayah et al., 2021). These instruments will be joined by the NASA-ISRO Synthetic Aperture Radar (NISAR) instrument and the European Space Agency's P-band synthetic aperture radar Biomass mission, dedicated to forest AGB mapping and both slated for launch in 2023.

While extant and upcoming orbiting lidar and radar instrument missions will improve the precision of AGB mapping and will also importantly extend the temporal and geographic coverage, the current record is limited. We would like to know the trajectories of AGB – accumulation from growth and losses from disturbance and human management – annually and across the southwestern U.S.. However, long forest AGB annual series are not currently available from active instruments and will not be available for at least another decade. The alternative is remote sensing from satellites that use passive solar wavelength sensors. These data have been used to map forest type, cover, and function at a range of scales, using surface spectral reflectance estimates and spectral vegetation indices as the primary metrics. However, none of these techniques are optimal for estimating AGB: the signal from measurements of reflected sunlight at medium (10–30 m) to moderate (100–1000 m) resolution is sensitive to plant condition and function; and to non-leaf components in the sensor field-of-view. Information on 3-D structure is thus confounded in the signal.

For regular observation at sub-annual to annual intervals and with regional to global coverage, the long-term record from passive instruments depends on three kinds of instruments: Those that have a large ground-projected instantaneous field-of-view (GIFOVs, i.e. moderate resolution) and wide swaths with varying observation geometries, e.g., MISR (~275 m), MODIS (~250 m); those that provide relatively limited angular information, e.g., ASTER on Terra (~15–30 m), ATSR-2 (~1 km), AATSR (~1 km); or those that only provide close-to-nadir spectral measures at medium spatial resolution, e.g., the Landsat series (~30 m). Of these, the moderate resolution imagers have received the most attention. For example, Blackard et al. (2008) used U.S. Forest Service Forest Inventory and Analysis (FIA) program ground measured inventory data for the conterminous U.S., Alaska, and Puerto Rico with MODIS data to develop empirical models to relate field-measured response variables (including AGB) to plot attributes and scale these up. However, nadir-spectral and single view angle remote sensing measures do not capture AGB directly as they are relatively insensitive to the structural component of canopies: again, the signal from structure is confounded with that from greenness (Diner et al., 1999; Qiu and Zhang, 2020).

In this study we pursue a multi-angle approach to mapping forest AGB that seeks to exploit the structural effects of canopies on observed radiation fields in the red wavelengths. This is achieved by exploiting the relationship between AGB and a suite of red band reflectance values simulated at different viewing angles, to develop a ratio-based index that is relatively insensitive to inter-annual changes in forest greenness from varying precipitation. Multi-angle bidirectional reflectance factor (BRF) data contain information about canopy structure because the proportions of sunlit and shaded tree crown and background in the instrument ground-projected instantaneous field-of-view (GIFOV) vary (Chen et al., 2003, Heiskanen, 2006, Li and Strahler, 1985, Schull et al., 2007, Wang et al., 2011). Observing in the solar direction there is an increasing proportion of shaded crown and background in the GIFOV with increasing zenith angle (i.e., illuminated elements are occluded), while the inverse is true when viewing in the antisolar, or backscattering, direction (i.e., shaded elements are occluded). Here, we first develop a multi-angle index to estimate forest AGB. This approach was developed because there are no physically-based remote sensing methods that provide wall-to-wall AGB mapping over this region, inter-annually, and from the year 2000. We then evaluate performance against lidar-based estimates from the NASA Carbon Monitoring System (CMS). Finally, we apply the method to the generation of AGB map series that reflect the major disturbances impacting these forests, verify that these correspond to published data, and quantify changes for States and major wildfire events.

2. Methods

The region to be mapped in this study encompasses the southwestern United States (California, Arizona, New Mexico, Colorado, Nevada, Utah, and parts of Wyoming and West Texas; Fig. 1), some 3,035,346 km^2 in total, including upland forest, desert grassland with significant woody shrub encroachment, and riparian woodlands. The primary data are from the NASA, Jet Propulsion Laboratory's Multi-angle Imaging Spectro-Radiometer (MISR) instrument flown on Terra, the first of NASA's Earth Observing System satellites that was launched on December 18, 1999 (Diner et al., 1999, 2005). MISR has nine pushbroom cameras arranged to view in a 360 km swath along-track and thus acquires image data with nominal view zenith angles relative to the surface reference ellipsoid of 0.0°, ±26.1°, ±45.6°, ±60.0°, and ±70.5° (forward and aft of the along track of the Terra satellite) in four spectral bands (446, 558, 672, and 866 nm) at 1.1 km spatial resolution. The 672 nm (red) band images are also acquired with a nominal maximum cross-track ground spatial resolution of 275 m in all nine cameras and all four bands are acquired at this resolution in the nadir camera (Diner et al., 1999). The cameras are denoted DF, CF, BF, AF, An, AA, BA, CA, DA, from most extreme forward-viewing (DF) though nadir (An) to most extreme aft-looking (DA; the off-nadir cameras are sometimes written Df, Cf…, and so on). The swath is approximately 380 km and the repeat period is nine days at the equator and 2 days at the poles (see Diner et al., 1999 for further specifics on the MISR sensor; animations of MISR's viewing are available at https://visibleearth.nasa.gov/images/53628/misr-scanning-swath).

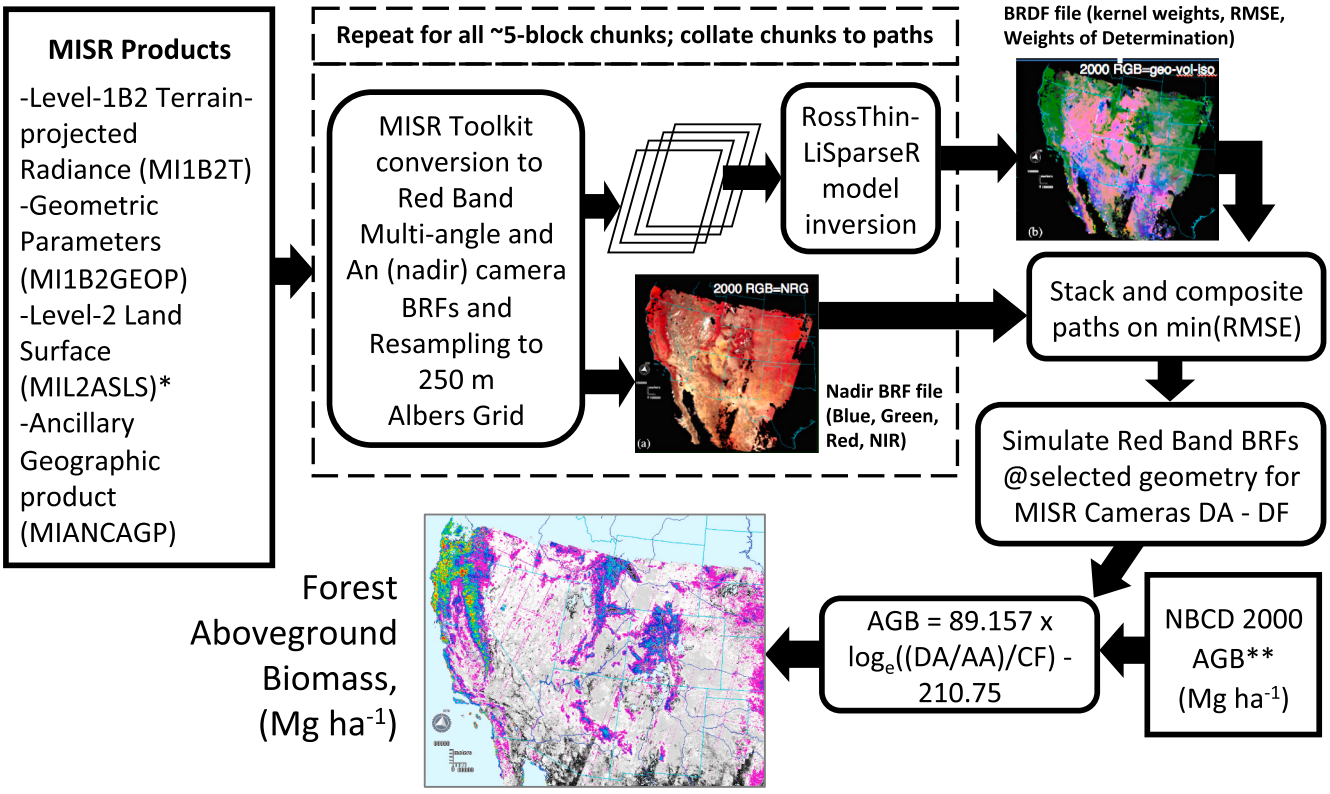

Fig. 1. MISR and AGB input data (square boxes) and operations performed (rounded boxes) in order to produce AGB maps using the multi-angle index approach. The AGB model given here was derived for a test area. *New v22b24–80 + 2 Interim Land product using revised aerosol optical depth retrieval at 4.4 km resolution. **National Biomass and Carbon Dataset, or other source of AGB calibration data (e.g., lidar-based from airborne and space-based platforms).

2.1. MISR data set preparation – surface BRF calculation and resampling

MISR Toolkit routines developed after suggestions by John Martonchik (Jet Propulsion Laboratory, 2020a) were used to project 275 m MISR surface BRFs on a 250 m Albers Conical Equal Area grid centered on intervals of 250 m (i.e., coordinates end with 000, 250, 500, or 750). BRF is obtained in these routines by performing a linear regression of the red band 1.1 km MISR surface BRFs against the red band 1.1 km MISR top-of-atmosphere BRFs in the Land product. Top-of-atmosphere BRFs contaminated by sun glint over water surfaces are not used in the regression calculation. Smoothed regression coefficients are subsequently applied to the red band 275 m top-of-atmosphere MISR BRFs to produce red band 275 m land surface BRFs for all cameras. The Toolkit procedures use the MISR Level-1B2 Terrain-projected Radiance product (MI1B2T), the MISR Level-1B2 Geometric Parameters product (MI1B2GEOP), the MISR Level-2 Land Surface product (MIL2ASLS, surface BRFs at 1.1 km), and the Ancillary Geographic product (MIANCAGP). The MI1B2T product provides 275 m terrain-projected top-of-atmosphere radiance in all 4 spectral bands for the nadir view, and in the red band for off-nadir views. Sun and view angles from the MI1B2GEOP product are combined with a land/water mask from the MIANCAGP product to determine view angles and surfaces susceptible to sunglint.

For May 15 – June 15 of each year, the An (nadir) camera BRFs in the 446, 558, 672, and 866 nm (blue, green, red, and near-infrared (NIR)) bands, and the red band BRFs in all cameras were processed to provide surface BRF for paths 29–47 within the region and resampled to the 250 m Albers grid. This was done using the v22b24–80 + 2 interim version of the 1.1 km Land Product, obtained using a revised 558 nm aerosol optical depth retrieval at 4.4 km resolution (Fig. 1). A smoothing algorithm was applied to the aerosol optical depth, reducing noise, and filling some gaps where aerosol retrievals are missing (*Jet Propulsion Laboratory*, 2016). The input data are thus very close to those that would be obtained using the new v23 MISR aerosol algorithm (Jet Propulsion Laboratory, 2020b). The data extraction and processing had to be effected in sets of up to seven blocks as the HDF-EOS protocol imposes a memory constraint. The An camera BRFs and the BRDF model inversion outputs (see §2.2 below) were collated from these sets of blocks to paths and the latter were stacked. Temporal compositing was then performed on the stacked path data sets, using the minimum BRDF model-fitting Root Mean Square Error (RMSE) value as the criterion to select for each location the observation least likely to be contaminated with cloud. The May – June period was chosen because at this time of the year woody plants have leafed out but grasses, forbs and other understory plants are often still dormant.

2.2. MISR data set preparation – BRDF model inversion and compositing

The RossThin-LiSparse-Reciprocal BRDF model predicts BRF at any given combination of viewing and illumination angles on the basis of three parameters, or "kernel wrights", that collectively describe surface reflectance anisotropy. It was adjusted against all available red band BRFs acquired May 15 – June 15 of each year from 2000 through 2015. Over the Rocky Mountains, the retrieval period was extended to the end of June in an attempt to compensate for persistent cloud obscuration and snow cover in forested areas with complex topography. This BRDF model was developed as one of the family of Ross-Li kernel-driven BRDF models by Wanner et al. (1995), based on the earlier ideas and model development work of Roujean et al. (1992), Li and Strahler (1985), and Walthall et al. (1985). The version with the RossThin kernel was selected as it is more appropriate for sparse canopies, with fewer negative kernel weights retrieved than with the RossThick kernel (Wanner et al., 1995). The model's isotropic (*iso*), geometric (*geo*), and volume scattering (*vol*) kernel weights were obtained by adjustment against MISR red band BRFs in all cameras, with the objective the minimization of the absolute RMSE.

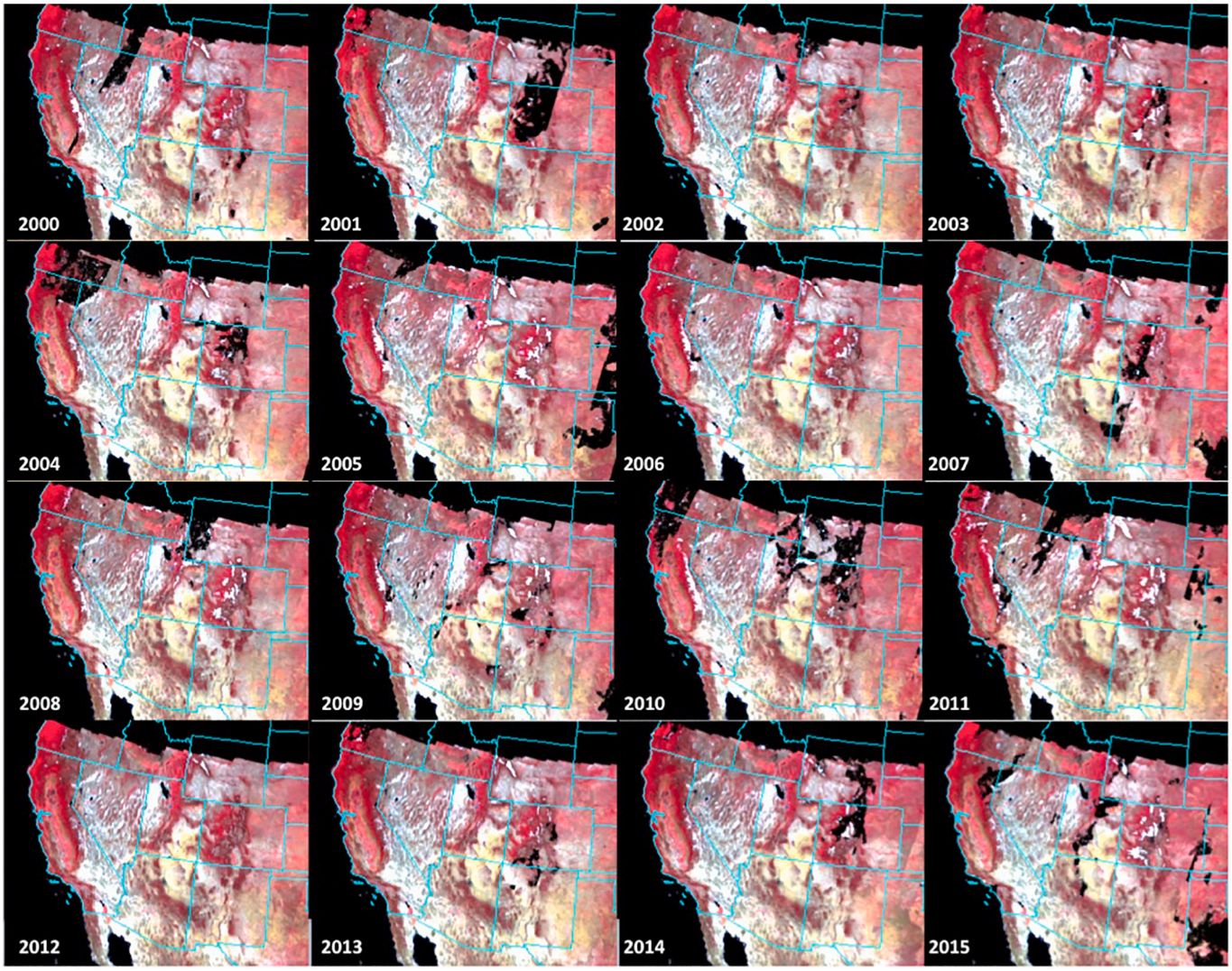

Fig. 2. MISR An (nadir) camera RGB = NRG false color composites for 2000–2015, constructed using data from May 15 through June 15, except for paths/blocks over the Rockies that used all data to the end of June. The gaps in the data sets can be largely filled by extending the compositing period to end-June for all paths and blocks. The compositing criterion was min(RMSE), where RMSE is the error on RossThin-LiSparse-Reciprocal BRDF model fitting.

Composited An (nadir) camera standard false color composites (RGB = NIR, Red, Green) show the extent of the available data (Fig. 2). There are clearly areas that do not have coverage in all years, notably parts of the Rocky Mountains in Colorado and southern Wyoming, as a result of persistent cloud and snow cover, as well as topographic obscuration. This is also shown in Fig. 3 for the year 2014, as an example. The earliest MISR data (for the year 2000) were used in calibrating an AGB prediction model by adjusting a coefficient against reference data. This model will be invalid for locations where MISR data for May 15 – June 15, 2000 are missing; and this will be propagated through the predictions for all years. However, it was not necessary to deal with this issue immediately in this study because the areas with missing data for the year 2000 do not include forested lands.

2.3. Creation of modeled MISR BRF datasets

Multi-angle red band BRF ratios are sensitive to forest canopy structure (Fig. 4 (a) and relatively insensitive to vegetation canopy foliage greenness – that varies importantly from year to year in dry regions such as the southwestern U.S. – and thus might be used to estimate forest AGB. However, multi-angle ratios require observations in all cameras used but data from all nine MISR cameras are not always available, owing to cloud or topographic obscuration. This is overcome through BRF modeling, by using the temporally-composited kernel weights to drive the BRDF model. Forward modeling was thus performed for all locations in the composited data set using the RossThin-LiSparse-Reciprocal BRDF model and the retrieved kernel weights. Red band BRFs were modeled for three geometries: in the mean MISR geometry for the region at the mean solar zenith angle at the center of the region; and in a solar principal plane (SPP) geometry (the same viewing and solar zenith angles but with relative azimuth angles of 0 and 180 degrees for the back- and forward-scattering hemispheres, respectively, referred to as $MISR_{spp}$); and in the SPP but with hot-spot and specular view zenith angles.

There is inevitably some error from extrapolation to unobserved geometries but this is probably quite small as it is somewhat mitigated by the semi-physical nature of the BRDF model (Strahler et al., 1996; Lucht and Lewis, 2000; Chopping, 2001). Weights of determination (noise amplification factors) for Normalized BRDF-Adjusted Reflectance (NBAR) with a constant solar zenith angle of 45° for initial calibration sites are given in Table A1; the WoDs for the modeled BRFs are likely to be lower, since the solar zenith angle used in modeling is closer to the typical observed one.

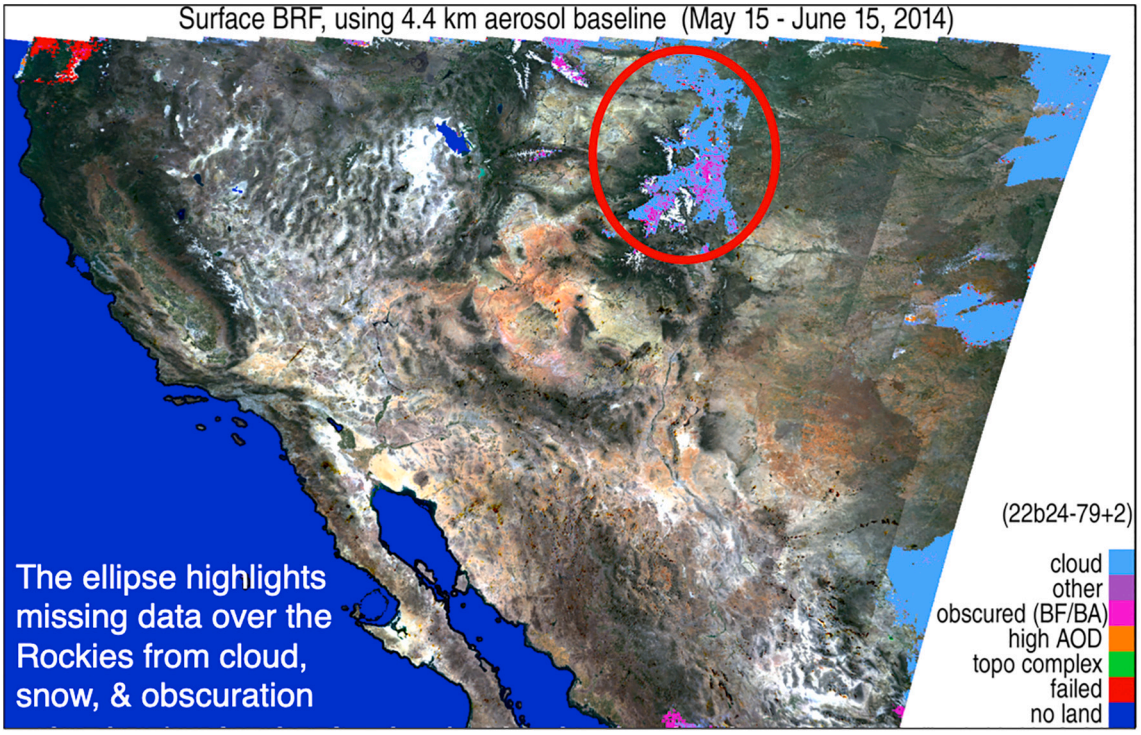

Fig. 3. MISR An (nadir) camera RGB color composite for May 15 – June 15, 2014. The red ellipse highlights missing data over the Rockies from cloud, snow, and obscuration. (For interpretation of the references to color in this figure legend, the reader is referred to the web version of this article.)

2.4. AGB prediction with a multi-angle index

Examination of modeled BRFs for a forested landscape in the vicinity of Mount Lindsey, Colorado allowed the derivation of a multi-angle index that has a $\log_e$ relationship with AGB. This area was selected because it covers a range of conditions and surface cover types (needleleaf forest, broadleaf woodlands, grassland, irrigated crops, snow, exposed rock, desert, surface water); and because AGB is generally more difficult to estimate at the lower end of the domain: if an approach is able to estimate AGB accurately here it might provide better estimates across the domain. False color composites were generated using modeled red band BRFs for various angular combinations and subsequently examined. An RGB = BA, AF, DA camera BRF (SPP) combination appears to reflect forest density (Fig. 4 (a), (b)). Plots were made of BRF values for locations with different forest AGB values (from NBCD 2000), as well as other cover types (Fig. 4 (c), the latter to determine whether MISR-based AGB estimates are unreasonable for crops, water, desert, and snow. Site details given in Table A1. These plots demonstrate that the shapes are dissimilar for different cover types, but also that there may be a relationship between AGB and BRF ratios. The BRFs cannot be used directly as predictors of AGB, since brightness variation is driven more by green vegetation cover than by tree density and height: this would inevitably lead to poor prediction potential (as shown in Fig. 7). Therefore, a number of red band BRF ratios and their relationships with NBCD 2000 AGB were explored, using a combination of backscattering-to forward-scattering BRFs. The ratios depend on canopy stem density and crown size that jointly determine the crown and background fractions in the instrument's GIFOV. The ratio of a slope of a pair of aft camera BRFs to a high zenith angle forward camera BRF – such as (DA/AA)/CF – provided a promising candidate (Fig. 5).

Plots of the multi-angle index (MAI) using the (DA/AA)/CF BRFs and the corresponding NBCD 2000 AGB values for a set of 21 locations for which the AGB values cover the domain seen in this area show that there is a moderately weak $\log_e$ relationship (R^2 = 0.53, Fig. 6 (b)). The relationship is weakened by two outliers but on examination of these locations in high resolution imagery it was apparent that they have large proportions of exposed bright rock (Fig. 6 (c) and (d)). If outliers are removed, the relationship is stronger (R^2 = 0.91, Fig. 6 (a)). Examining these relationships for three candidate indices generated with red band BRFs modeled at three geometries, (DA/AA)/CF was the best index and was selected for further study (Table 1). The MAI derivation is given in Eq. (1)., noting that this was initially generated for three geometries:

$$\mathrm{MAI} = (\mathrm{DA}/\mathrm{AA})/\mathrm{CF} \quad (1)$$

The utility of the relationship between a multi-angle index and NBCD 2000 AGB is highlighted by attempts to just use spectral-nadir metrics for the same purpose for the 19 screened Mt. Lindsey forest sites. MAIs based on (DA/AA)/CF at any of the three geometries showed strong relationships with NBCD 2000 AGB (R^2 = 0.90 to 0.91, RMSE = 17, 21, and 19 Mg ha^{-1}, respectively), while more common NDVI, red BRF, and NIR BRF all showed weak relationships (R^2 = 0.32, 0.07, 0.37, respectively, RMSE = 119, 120, and 120 Mg ha^{-1}, respectively). It should perhaps not be surprising that the spectral-nadir metrics are not particularly closely related to forest canopy density in environments where soils are mineral-dominated with low organic matter content and thus as bright in the NIR region as green vegetation, reducing the utility of common spectral reflectance indices such as NDVI.

The selected model is therefore

$$\mathrm{AGB}\left(\mathrm{Mg\ ha^{-1}}\right) = 89.16 \times ln(\mathrm{MAI}) - 210.75 \quad (2)$$

where the MAI is henceforth defined as in Eq. (1) with BRF modeling in the SPP. This was applied to all locations across the entire southwestern US and predictions for 1968 random points were extracted and compared with NBCD 2000 values (Fig. 8). This demonstrates that, unsurprisingly, a single unique model (or set of coefficients) is inadequate for accurate AGB mapping, since there are variations in forest type, soils, and topography across the region.

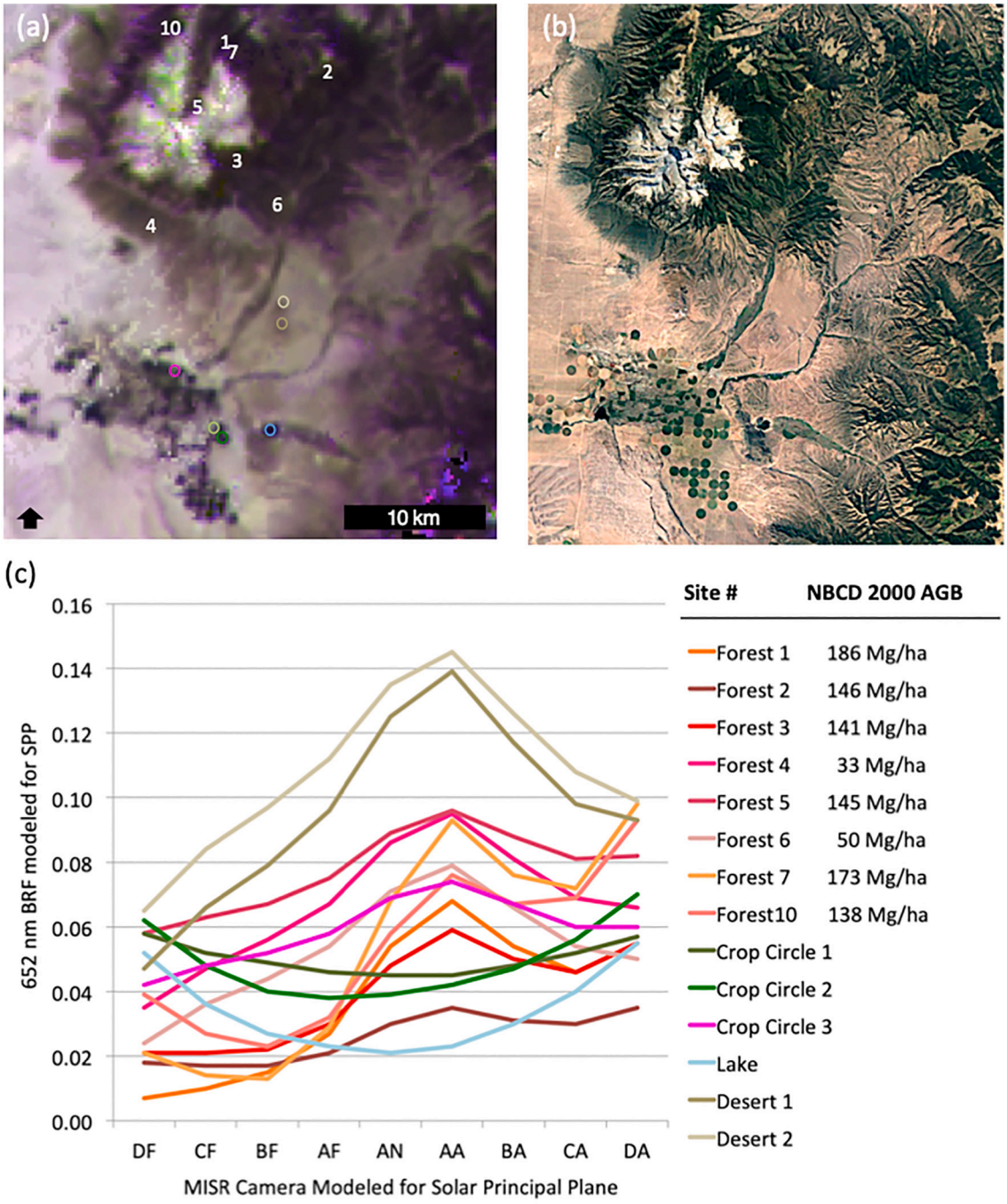

Fig. 4. (a) MISR color composite overview for Mt. Lindsey, CO, from SPP red BRFs with R, G, B = BA, AF, DA cameras, with dense forest appearing in deep purple. Locations of forest sites are numbered; other sites listed in (c) are color-coded (b) Google Earth pan-sharpened true color imagery for the same area (c) MISR SPP red BRFs for various land covers with NBCD 2000 AGB for forest sites. (For interpretation of the references to color in this figure legend, the reader is referred to the web version of this article.)

2.5. Enabling region-wide mapping

Since a unique model coefficient and intercept set are insufficient for the mapping of AGB for all locations across the southwestern United States, a method had to be derived to account for the effects caused by differences in terrain, forest type, and soils. The first step was to examine an area for which there are multiple CMS data sets: the Rim Fire area, in the Sierra Nevada of California. The data sets include two lidar-based AGB maps, one at 35 m from a 2013 airborne lidar survey (ALS) that used allometric equations based on lidar-derived heights at tree and plot levels (Xu et al. (2018a)); and one for 2005 for the entire western US at 100 m, from ICESat Geoscience Laser Altimeter System (GLAS) data, trained with FIA data (Hagen et al., 2016; Harris et al., 2016; Sassan Saatchi, pers. comm).

To account for the differences in terrain, forest type, and soils, the $\log_e$ model can be fitted to the NBCD 2000 AGB data by adjusting the coefficient and intercept using numerical methods, i.e., minimizing the root of the average of squared differences with year 2000 MISR-derived AGB and NBCD AGB across all data, i.e., minimizing the objective given in Eq. (3):

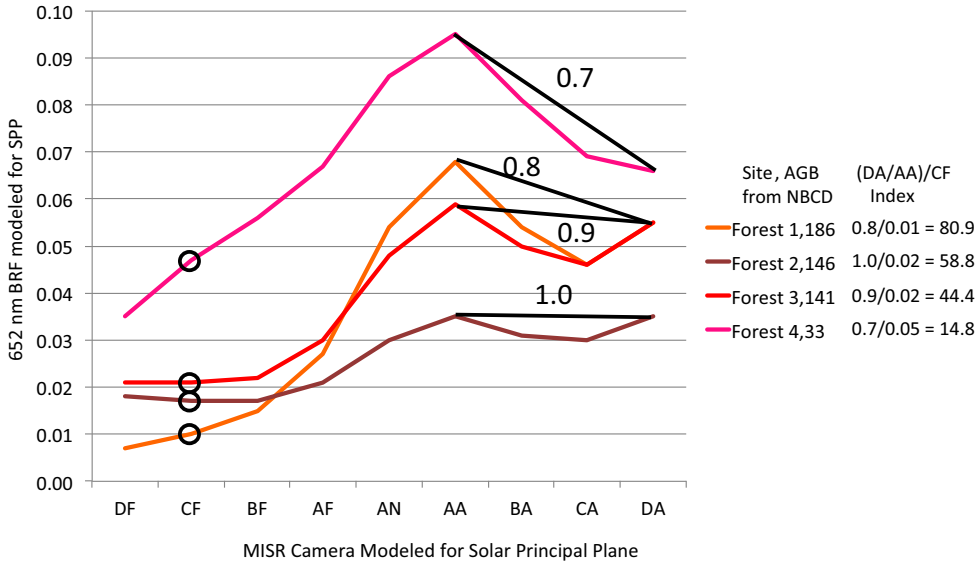

Fig. 5. MISR simulated red band BRF plot showing how a multi-angle index that predicts AGB can be calculated (example for four sites with very different AGB values). (For interpretation of the references to color in this figure legend, the reader is referred to the web version of this article.)

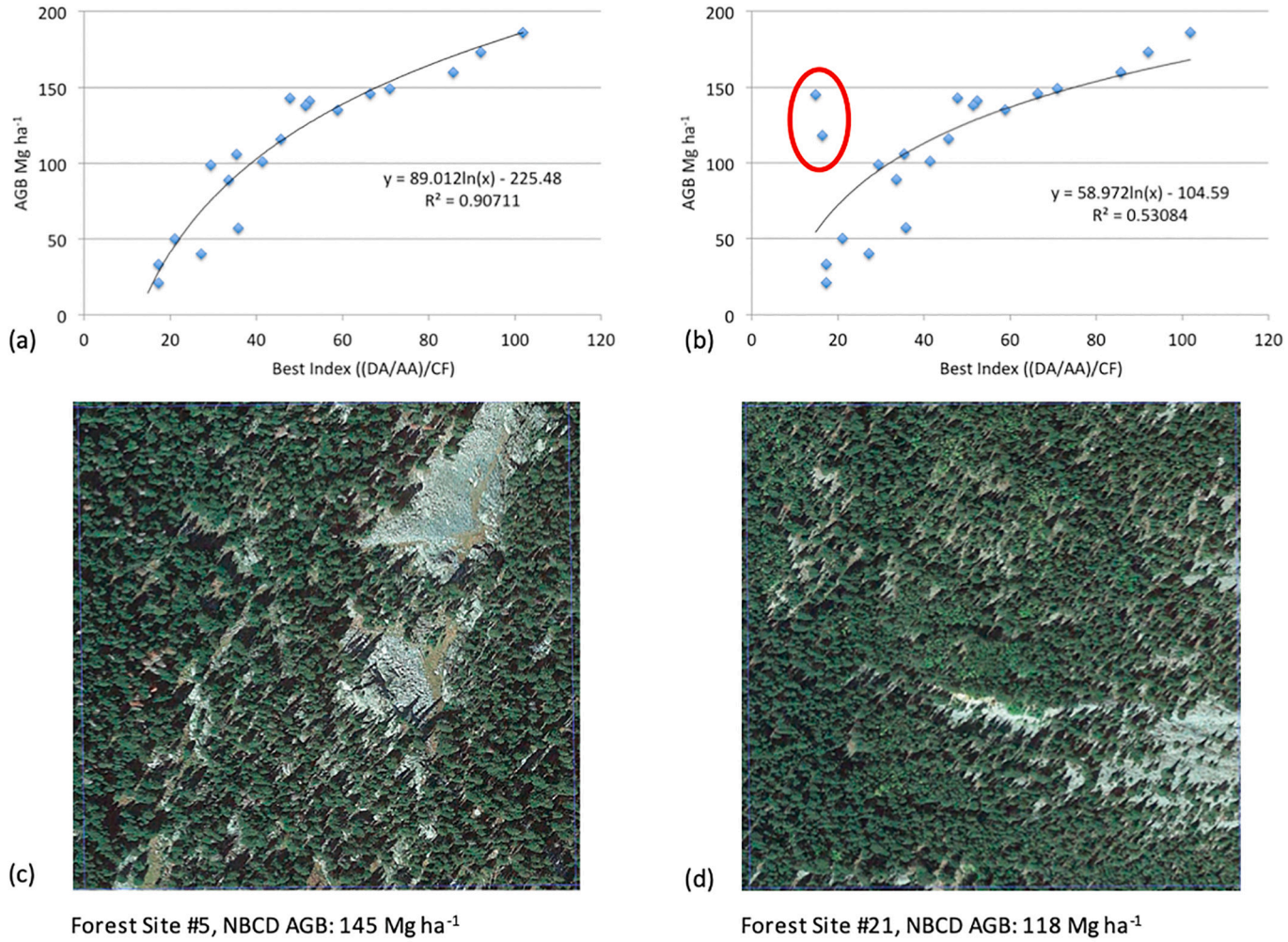

Fig. 6. (a) Multi-angle index with sites #5 (NBCD = 145 Mg ha^{-1}) and #21 (NBCD = 118 Mg ha^{-1}) removed (b) the same plot including these sites, indicated with a red ellipse (c) and (d) Google Earth imagery for these sites, respectively. Imagery: Google Earth/Maxar. (For interpretation of the references to color in this figure legend, the reader is referred to the web version of this article.)

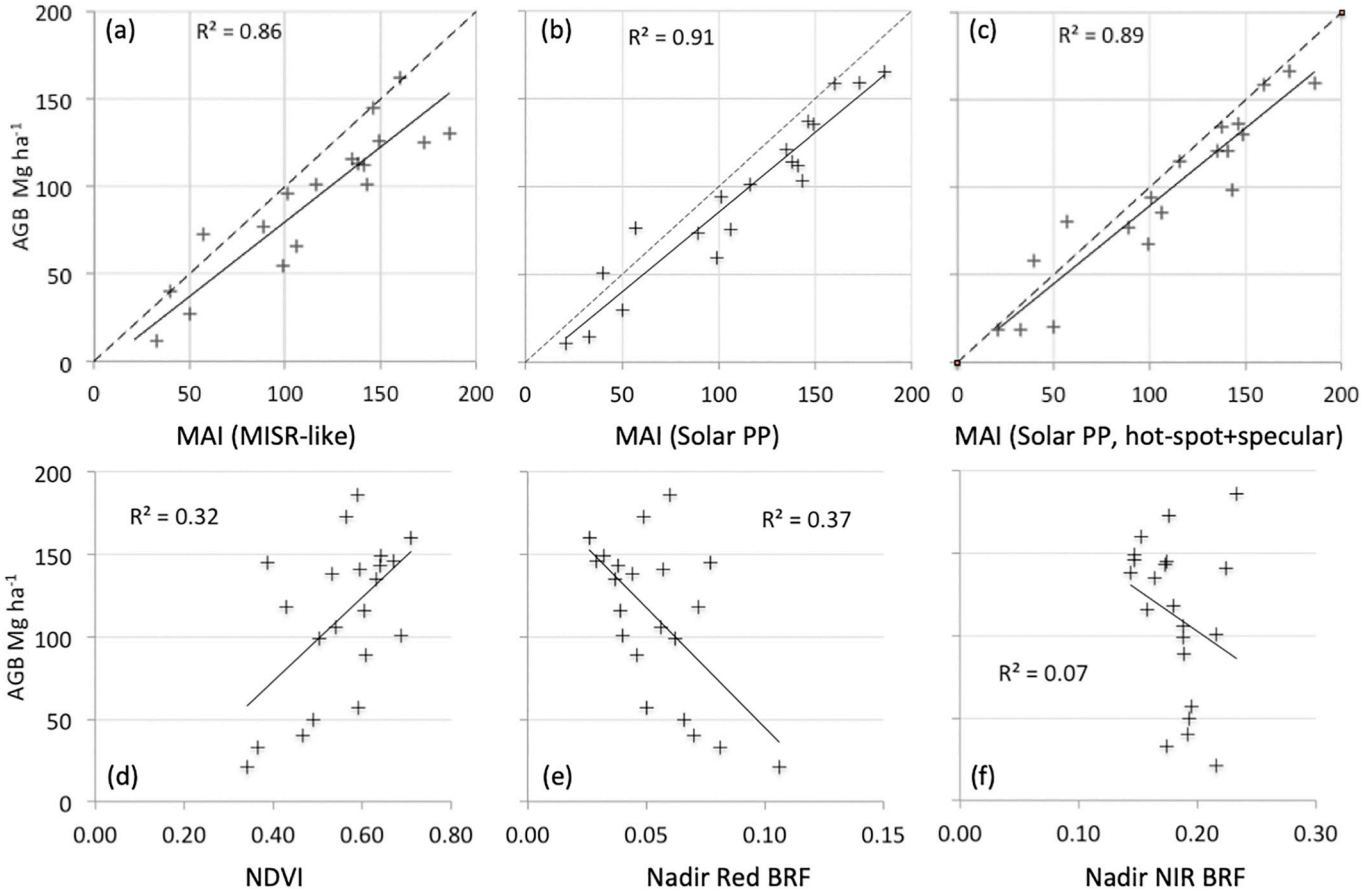

Fig. 7. Relationships between NBCD 2000 AGB and (a) the (DA/AA)/CF multi-angle index, in MISR-like viewing directions (b) ditto, in the solar principal plane (c) ditto, with hot-spot and specular directions (d) NDVI calculated with the MISR An camera red and NIR BRFs (e) MISR An camera red BRFs (f) MISR An camera NIR BRFs. All data are for the year 2000. (For interpretation of the references to color in this figure legend, the reader is referred to the web version of this article.)

$$RMSE = \sqrt{\frac{1}{n}\sum (AGB_{MISR} - AGB_{NBCD})^2} \quad (3)$$

However, with two unknowns there are many possible solutions, so the model in Eq. (2) must be reduced to Eq. (4):

$$modeled\_AGB = a \times log_e(MAI) \quad (4)$$

Creating a coefficients map for the entire southwestern using extrapolation is not feasible because soil and understory conditions, topography, and forest types vary considerably across the region. Therefore, the commonly used Brent optimization approach (Brent, 1973) was used with the model and year 2000 $MISR_{spp}$ data to obtain the *a* coefficient for every location on the 250 m grid by fitting the model to the NBCD 2000 estimate by minimizing the RMSE in Eq. (3). This was accomplished using the code provided in Burkardt (2019). The resulting map of coefficients was used to predict AGB using the $MISR_{spp}$ MAI for all locations and all years, 2000–2015. Clearly, where there are missing data in the year 2000 MISR data set, the *a* coefficients for those locations will be invalid, impacting the AGB predictions for all subsequent years. However, these locations are almost entirely outside forested areas, so there is very little impact on the results presented here.

Table 1
Performance of three multi-angle indices calculated with red BRFS in three different geometries: MISR-like, MISR-like but in the solar principal plane, and the latter but with viewing in the hot spot and specular directions. Based on 21 sites in the vicinity of Mount Lindsey, Colorado.

Multi-Angle Index	Geometry	R^2 (index vs AGB)	R^2 (predicted AGB)	RMSE Predicted AGB	Predicted AGB for Crop Circle Mg ha^{-1}	AGB Prediction Function
	MISR	0.79	0.86	19.4	51	102.29 x LN(index) - 230.51
(DA/AA)/CF	Solar PP	0.84	0.91	15.4	106	89.157 x LN(index) - 210.75
	SPP-HOTSPOT	0.80	0.89	17.1	39	63.596 x LN(index) - 132.88
	MISR	0.82	0.88	17.1	42	101.96 x LN(index) - 251.00
(DA/BA)/CF	Solar PP	0.82	0.91	15.3	95	89.012 x LN(index) - 225.48
	SPP-HOTSPOT	0.79	0.90	16.5	39	63.266 x LN(index) - 143.39
	MISR	0.82	0.87	17.8	34	110.86 x LN(index) - 291.96
(DA/CA)/CF	Solar PP	0.78	0.88	17.0	80	93.188 x LN(index) - 252.72
	SPP-HOTSPOT	0.87	0.89	16.0	32	66.935 x LN(index) - 169.69

Note: AGB in the columns with R^2 refers to the NBCD 2000 AGB values.

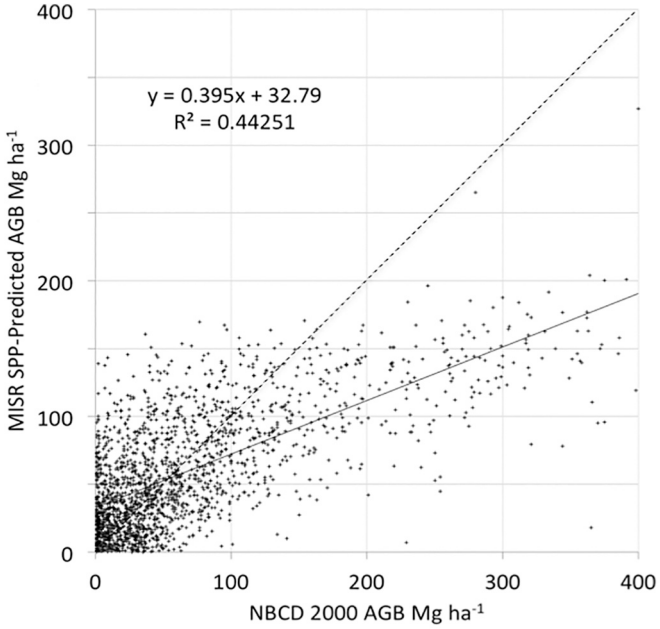

Fig. 8. Forest AGB Predictions for 1968 random points over the entire southwestern US with AGB = 89.157 × ln(MAI) - 210.75, where the MAI = (DA/AA)/CF from $MISR_{spp}$ BRFs. The dotted line = 1:1.

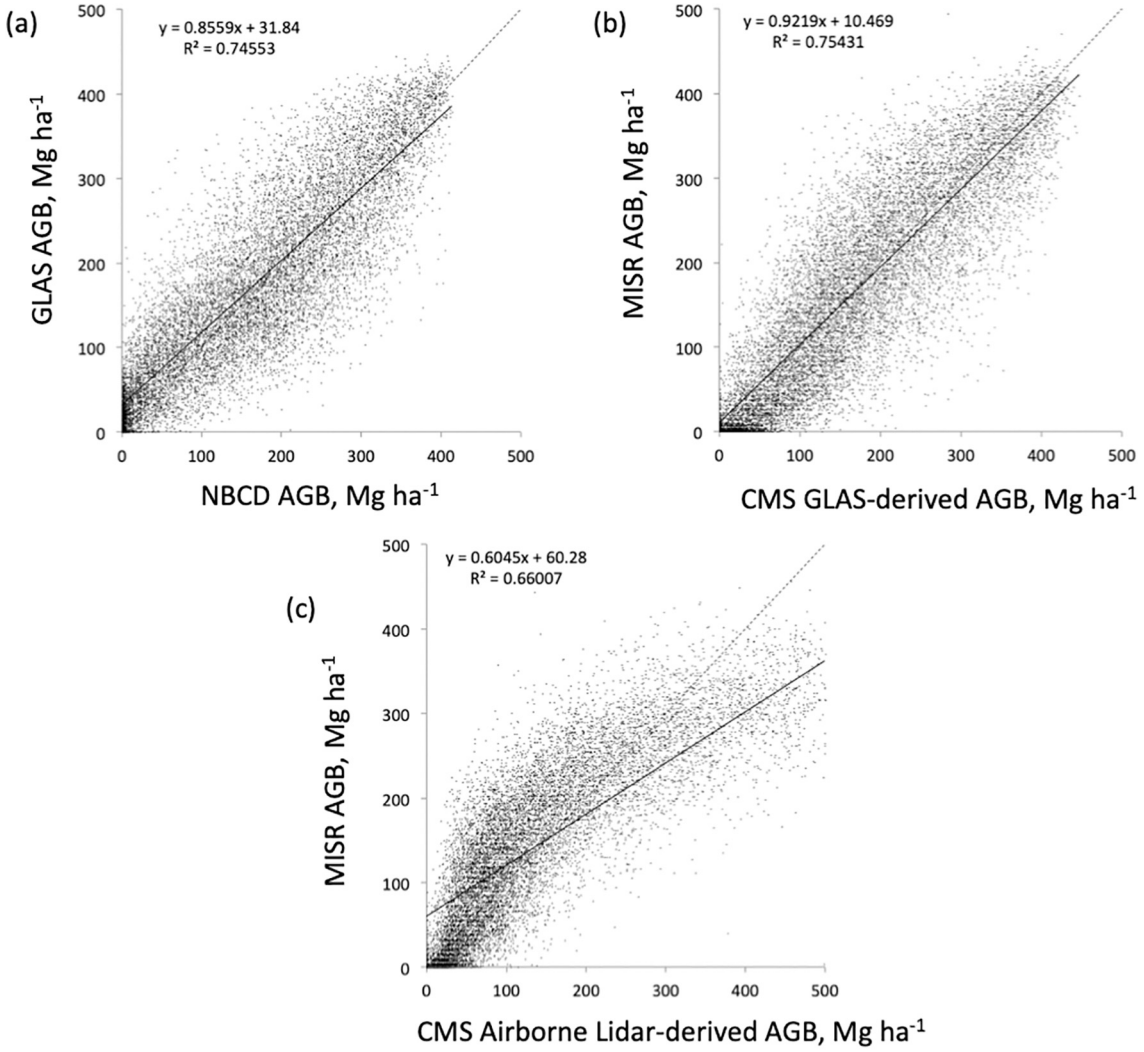

Fig. 9. Rim Fire area forest AGB at 250 m spatial resolution (N = 12,577: 100 × 126 locations, minus 23 locations where MISR data were missing). (a) GLAS-derived (2005) vs NBCD 2000 AGB (b) MISR (2005) vs GLAS (2005) AGB (c) MISR (2014) vs post-fire airborne lidar (2013) AGB. The lidar data sets were up-scaled to the 250 m grid using a zonal mean function. Solid (dotted) lines are trendlines (1:1).

3. Results and discussion

3.1. Assessment against NASA CMS datasets

The relationships between the MISR-predicted AGB and the upscaled CMS data sets for the Rim Fire area were reasonably strong, with coefficients of determination of 0.66–0.75; the correlation between the CMS GLAS (2005) and NBCD (2000) AGB was of similar magnitude ($R^2 = 0.75$) (Fig. 9, Table 2).

It is clear that the MAI-derived AGB has a slightly weaker and less consistent relationship with the AGB estimates based on the high resolution CMS ALS data, especially for higher biomass values. For the region >300 Mg ha^{-1} in the CMS data set, the MAI-derived AGB is underestimated with respect to the airborne lidar-based AGB. While it is known that large footprint lidar can overestimate tree heights in rough terrain as a result of ground displacement within the footprint (e.g., Breidenbach et al., 2008), plot-level estimates from small footprint lidar (e.g., ALS) have been shown to also underestimate AGB (Xu et al., 2018b, Clark et al., 2004). It is therefore acknowledged that the GLAS and ALS data sets are not entirely equivalent.

The spatial distributions of AGB in the NBCD (~2000), CMS- (2005), and 2003 MISR-derived maps are very similar, with no major discrepancies (Fig. 10). However, in earlier efforts to produce MISR-derived AGB map series using boosted regression tree models driven by BRDF model kernel weights, highly unrealistic trajectories were obtained, with AGB varying by large increments (e.g., ±100 Mg ha^{-1}) from year-to-year (Chopping et al., 2015, 2018, 2019). While one instance of this pattern might be interpreted as a single anomalous estimate, it was apparent that this kind of noise is persistent, with no straightforward correction method.

In these new results, trajectories were plotted against the CMS AGB data for 2005 and 2013 for a large number of locations and error statistics were calculated for all valid Rim Fire data ($N = 12{,}577$: 100 × 126 locations, minus 23 where MISR data were missing). The plots were visualized in an animation for the first 300 instances that is available at Vimeo (https://vimeo.com/480931672), showing that the trajectories are reasonably stable. The error in the MAI-derived AGB vs AGB from airborne and spaceborne lidar was normally distributed with a mean close to zero in both cases (standard deviations: 82.8 and 59.1, respectively; Fig. 11).

For analysis of the regionwide AGB maps, additional operations were necessary. To mitigate the impact of missing data and assess wall-to-wall changes in AGB regionwide over the period, the maps for 2000 and 2001 were combined, as were those for 2014 and 2015. Since missing data in the forest AGB maps were flagged with −1, maximum-value compositing was used to preferentially select a valid AGB prediction value over a missing data value. For mapping the net change in AGB over the period, missing or invalid data in the composites was flagged with −9999, since −1 is a valid AGB loss value.

Table 2
RIM fire area AGB comparisons: coefficient of determination and RMSE.

Data Sets	Years	R^2	RMSE
NBCD vs. GLAS	2000 vs. 2005	0.75	58.9
NBCD vs. ALS	2000 vs. 2013	0.61	88.7
GLAS vs. ALS	2005 vs. 2013	0.53	99.1
MISR vs. GLAS	2005 vs. 2005	0.75	59.2
MISR vs. ALS	2013 vs. 2013	0.61	92.8
MISR vs. ALS	2014 vs. 2013	0.66	82.8

Note: There is no point comparing the year 2000 MISR-derived AGB to NBCD 2000, since the latter was used to adjust the model's *a* coefficient for each location.

3.2. Assessment of regionwide mapping

Forest AGB maps spanning the southwestern U.S. from NBCD (2000), CMS (2005), and MISR (2005) show a similar spatial structure (Fig. 12). At this scale, discrepancies are hard to perceive, though there are some notable differences. For example, the MISR and CMS-GLAS maps show more extensive low AGB than the NBCD 2000 map, with the MISR estimates lying between CMS-GLAS and NBCD 2000 maps. Another difference is that the MISR-based map is missing data for some upland locations, for example, the Lincoln National Forest on the Sacramento Mountains of New Mexico, likely owing to cloud cover. For annual mapping this could be addressed in future efforts by extending the compositing period to the end of June for all locations – this had an important impact on the coverage over the Rocky Mountains in

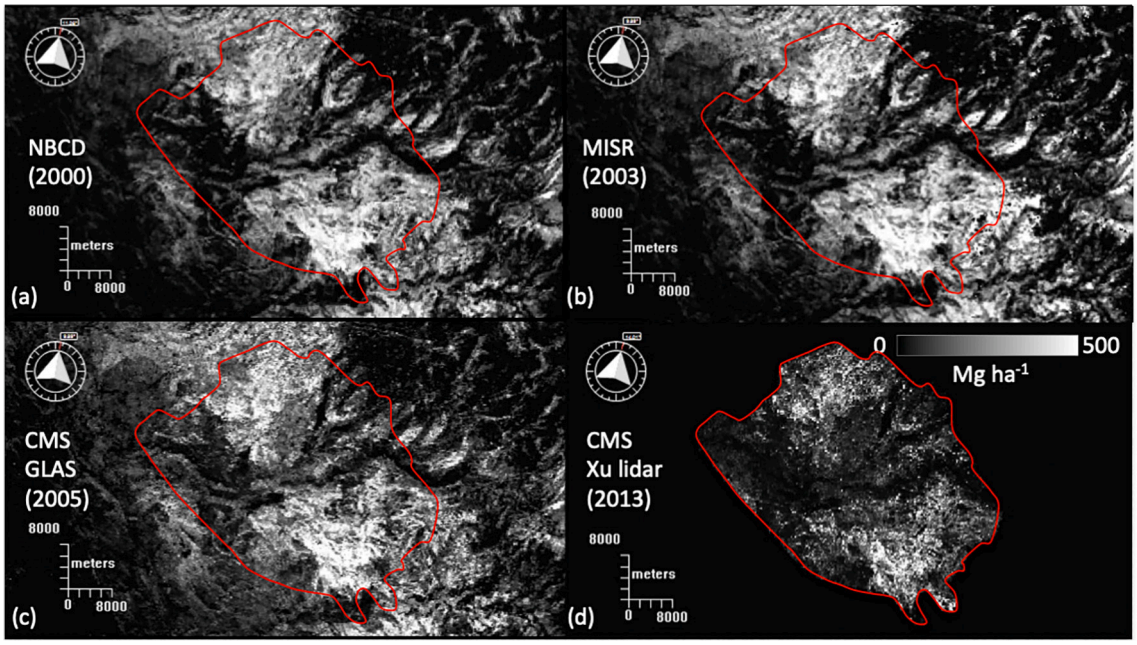

Fig. 10. Forest AGB density maps for the ALS Rim Fire area (red) (a) NBCD 2000 (b) MISR, 2003 (c) CMS GLAS, 2005 (d) CMS Xu ALS, 2013 (post-fire), black outside the boundary indicates "no data". (For interpretation of the references to color in this figure legend, the reader is referred to the web version of this article.)

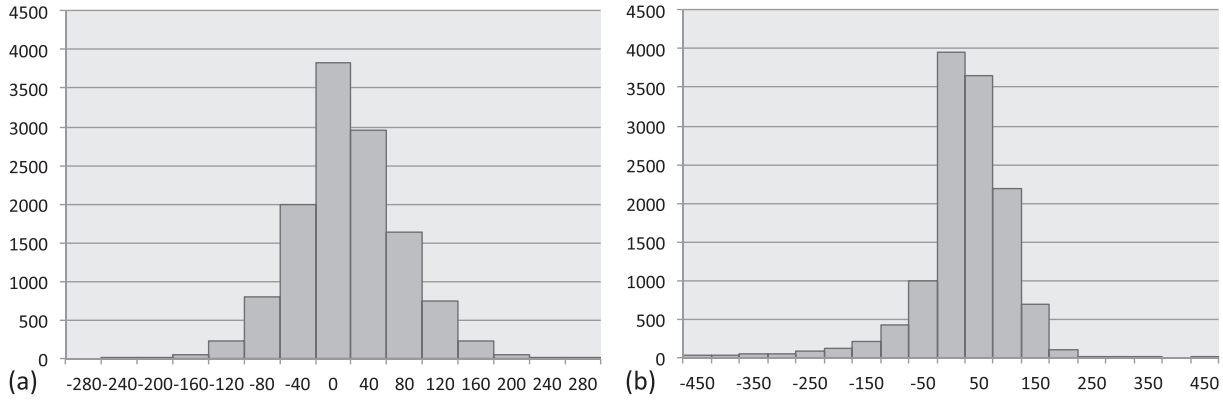

Fig. 11. Distribution of residuals for the $MISR_{spp}$ MAI-derived AGB vs AGB from (a) spaceborne and (b) airborne lidar. N = 12,577; standard deviations = 59.1 and 82.8, respectively.

Colorado and southern Wyoming – but for change assessment over the longer term, the estimates for the first two and the last two years can be combined, as described above.

The RMSE between the 2005 MAI-derived AGB vs estimates for the same year from ICESat GLAS trained with FIA data (N = 11,019,944, excluding missing and invalid flagged data) was 37 Mg ha^{-1}, with an R^2 of 0.9 The distribution of residuals (MISR minus GLAS estimates) was centered close to zero (Fig. 13), with Mode = 0.99; Median = 1.95; Mean = −3.63; and St. Deviation = 36.9.

3.3. Changes evidenced by the series

The net change in forest AGB calculated using the 2000/01 and 2014/15 composites shows that many areas have witnessed marked forest loss from wildfire and mountain pine beetle over the period, including the Uinta-Wasatch-Cache, Manti-La Sal, and Ashley National Forests in N. Utah; most of the forests of the Colorado Rockies; parts of the Sierra Nevada and Los Padros National Forest, Sespe Condor Sanctuary, and Angeles National Forest in S. California; the Arizona/New

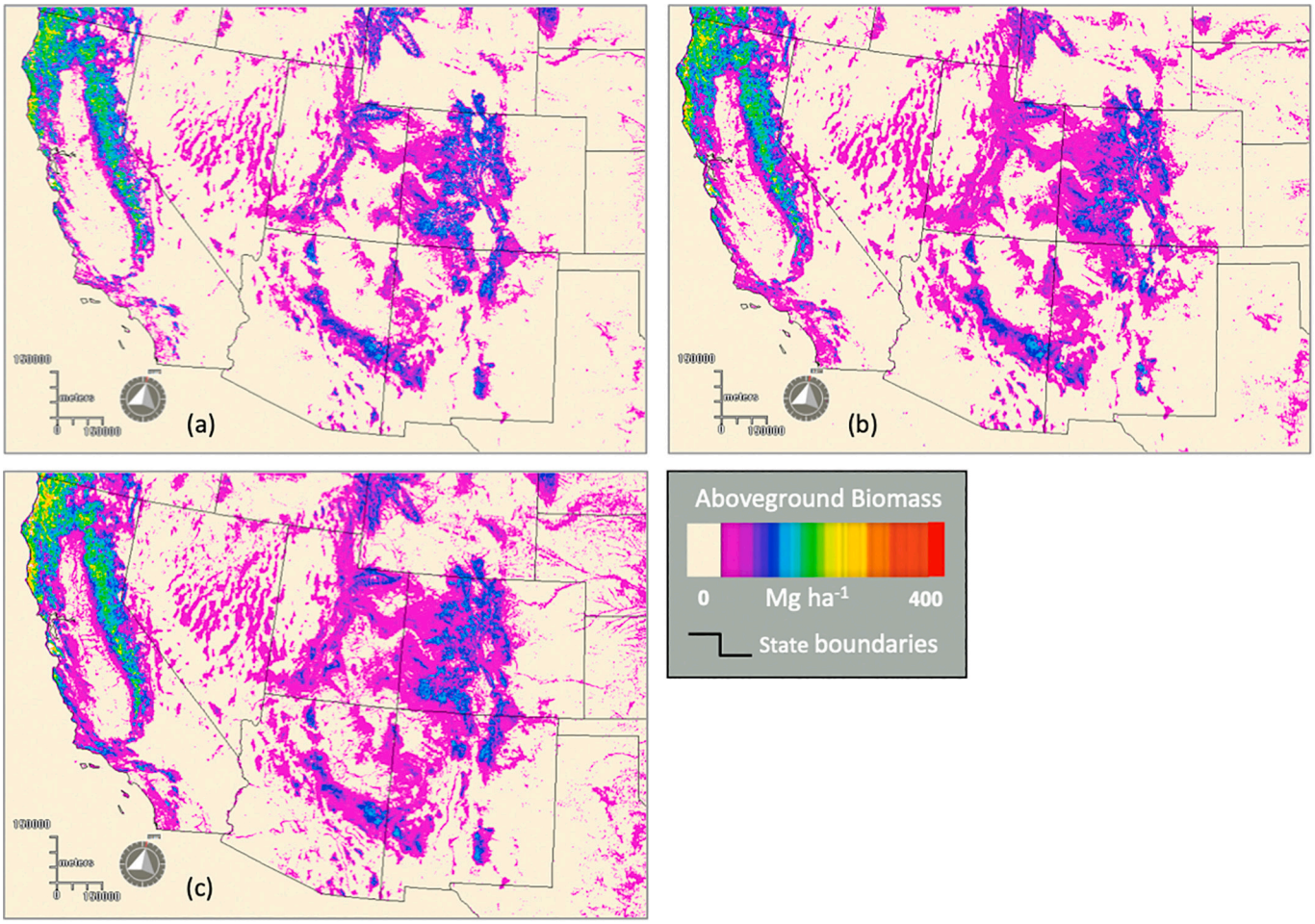

Fig. 12. Three AGB maps for the southwestern United States (a) NBCD 2000 (b) MISR 2005 (c) CMS GLAS-FIA 2005. Note that "zero" values indicate zero forest AGB, not zero woody plant AGB.

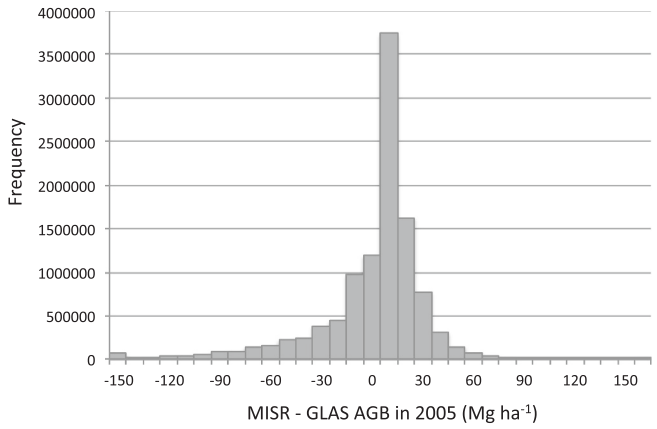

Fig. 13. Distribution of residuals (MISR minus GLAS) for the 2005 $MISR_{spp}$ MAI-derived AGB vs estimates for the same year from 2005 ICESat GLAS trained with FIA data, excluding missing and invalid flagged data.

Mexico Mountains ecoregion, and the S. part of the Sangre de Cristo Mountains in N. New Mexico. (Fig. 14).

Where disturbance has not been severe, the change map shows modest increases in forest AGB for many areas, with the largest in Klamath National Forest in N. California and Jackson State Forest in coastal California. Lesser increases are seen in the W. part of the Fort Apache Reservation in Arizona, the E. part of the Uncompahgre National Forest in *S. Colorado*, and throughout the Sierra Nevada range, from the Sierra National Forest in the south to the Tahoe, Plumas, Lassen, and Shasta-Trinity National Forests in the north.

Areas of important forest loss in the MISR-derived change map correspond well with fire and beetle loss perimeters from the GeoMAC Historic Wildland Fire Perimeters data set for the years 2001–2013 (Walters et al., 2011) and 2003–2012 (Berner et al., 2017a, 2017b), respectively (Fig. 15). The MISR-derived forest AGB net change map also shows areas affected by losses that do not appear in the wildfire perimeter or beetle loss maps; this is potentially because the losses occurred after 2012; but they may also reflect real changes (e.g. from forest harvest, thinning, or drought) that are not included in either of the disturbance map data sets (e.g., parts of Arizona's Galiuro Mountains, Fig. 15(b)).

Estimates of net forest AGB changes by state are given in Table 3, considering only locations for which there is valid data for both early and late AGB composites. Colorado saw the largest net loss in absolute terms, with forest AGB reduced by 10.1 Tg (−1.7%), while the largest relative loss (and second-highest absolute net loss) was sustained by New Mexico (−3.3%). California saw the largest net increase: 22.1 Tg (+1.2%), while Nevada saw almost no net change.

3.4. Forest biomass changes from MISR: wildfires

Estimates of net AGB losses for large contiguous forest fires delineated by GeoMAC fire perimeters are given in Table 4. The majority occurred after 2010, with only the Rodeo-Chediski (2002), Moonlight (2007), and Hayman (2002) fires occurring earlier. This is consistent with studies finding that wildfire has increased importantly in these

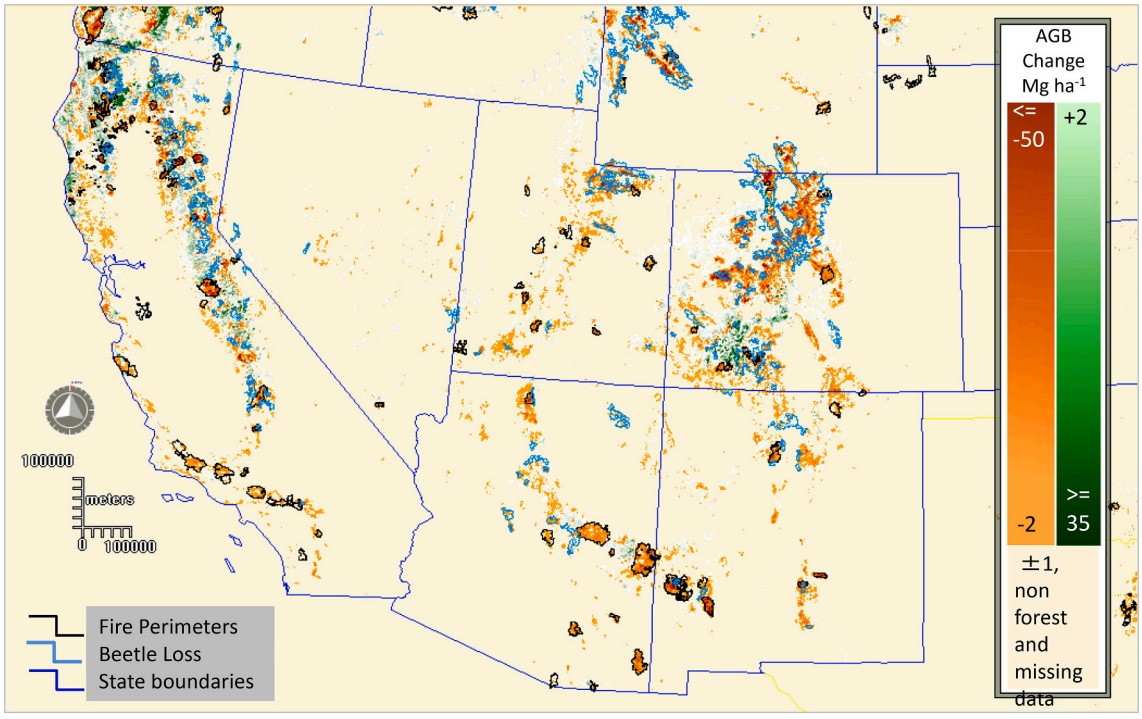

Fig. 14. Net changes in MISR-derived AGB density over the period (2014/15 minus 2000/2001) for the southwestern United States. Note that some forested areas are not included owing to missing data in either the earlier or later AGB composites. Fire perimeters are from the GeoMAC Historic Wildland Fire Perimeters data set for the years 2001–2013 (Walters et al., 2011), filtered to include only fires larger than 100 km^2 (25,000 acres) for clarity; fire perimeters on non-forest land were removed. Beetle loss areas for 2003–2012 are from Berner et al. (2017a), filtered to include only areas larger than 50 km^2 (12,355 acres).

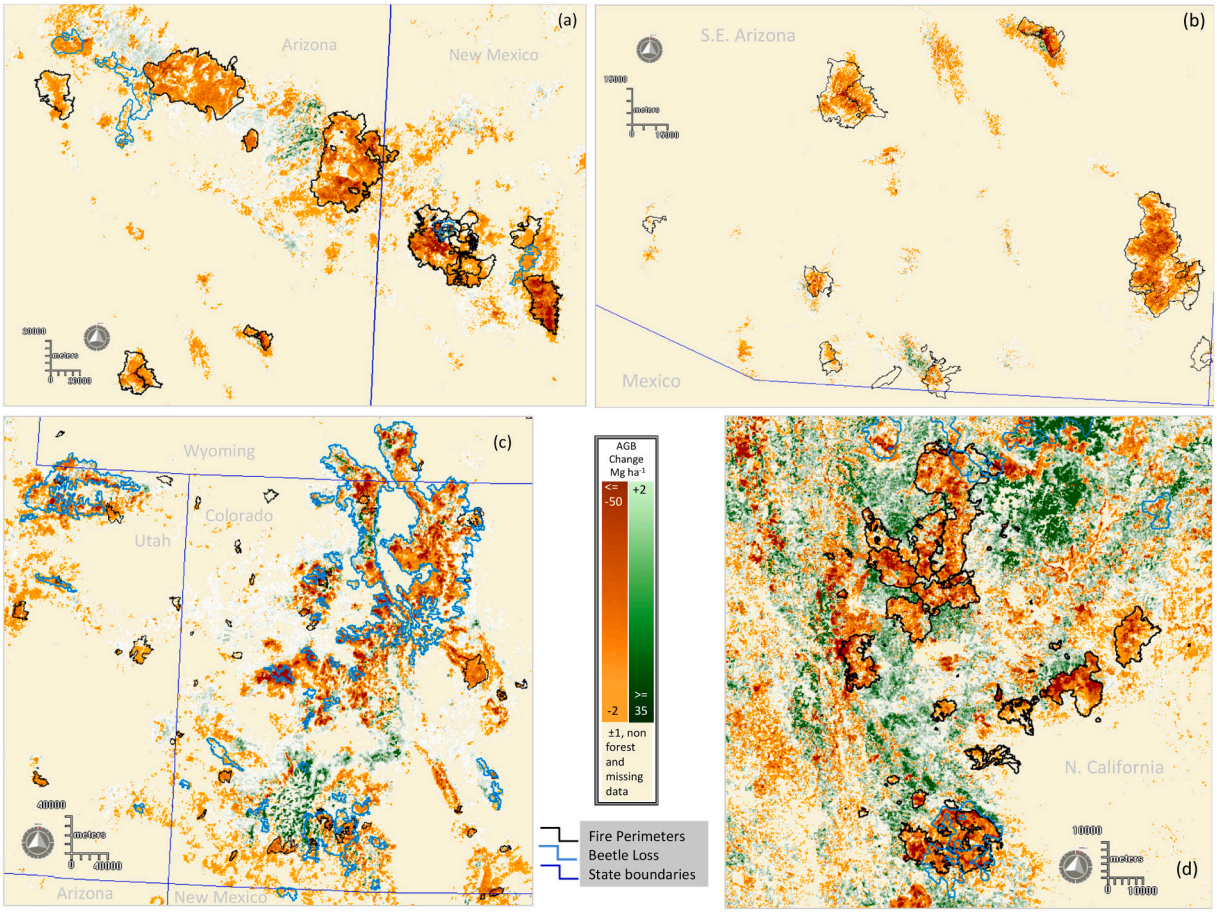

Fig. 15. Change in MISR-derived AGB density over the period (2014/15 composite minus 2000/2001 composite, units: Mg ha^{-1}. Detail for (a) E. Arizona (b) S.E. Arizona but with smaller fires also shown, (c) N. Colorado and parts of Utah and Wyoming, and (d) N. California (Lime Complex and Shu Lightning Complex on the W and E sides).

Table 3
Estimated forest AGB loss in 2014/15 over 2000/01, by state.

State	AGB 2000/01 (Tg)	AGB 2014/15 (Tg)	Net Change (Tg)	% Change	% Missing Data
Colorado	603.9	593.8	−10.1	−1.7	0.9
New Mexico	255.1	246.6	−8.5	−3.3	2.2
Arizona	267.4	261.4	−6.0	−2.2	0.0
Utah	266.4	261.2	−5.2	−2.0	0.3
Nevada	108.7	109.4	0.8	0.7	0.5
California	1872.8	1895.0	22.1	1.2	0.3

forests since the 1980s, with climate-related factors (such as warmer temperatures, drier summers, below-average winter precipitation, and earlier spring snowmelt) resulting in increased fire frequency, size, and severity (Dennison et al., 2014; Westerling, 2016; Abatzoglou and Williams, 2016; Williams et al., 2019). Fire events are clearly reflected in AGB trajectories for locations inside historical fire perimeters, with some of the largest happening later in the period (Fig. 16).

3.5. Forest biomass changes from MISR: beetle

Mountain pine beetle has resulted in large forest losses through tree mortality in many areas from the Sierra Nevada to N. Utah and parts of New Mexico and Arizona but is especially evident in Colorado and S. Wyoming (Fig. 17). MISR-derived AGB losses for affected contiguous areas identified in Berner et al. (2017a) are considerable at 16.6 Tg, with a single extensive area of 13,262 km^2 in the E. Rockies (#1 in the figure) accounting for almost 60% of the total, followed by a much less extensive but more severely affected area in Grand Mesa National Forest (#2).

Table 4
Estimated forest AGB loss in 2014/15 over 2000/01 for large contiguous fires in the southwestern united states, by size of loss.

Fire Year, State and ID#	Fire Name	Forest fraction[1]	AGB Loss (Mg)	Map Subset
				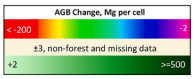
2011-AZ-ASF-F4CX	Wallow	0.87	1,998,253	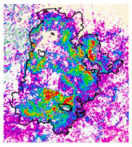
2013-CA-STF-HV2F	Rim	0.66	1,714,897	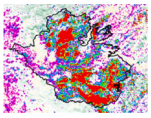
2002-AZ-FTA-251	Rodeo - Chediski	0.92	1,457,791	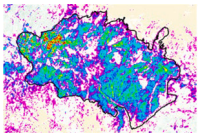
2013-NM-GNF-HJ20	Silver	0.94	1,251,173	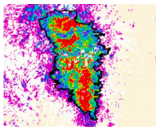
2012-NM-GNF-GU3S	Whitewater Baldy Complex	0.90	1,132,166	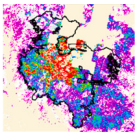
2012-CA-PNF-G32E	Chips	0.79	873,880	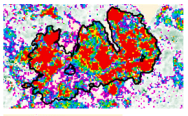
2011-AZ-CNF-F3KV	Horseshoe 2	0.72	826,778	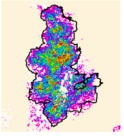
2007-CA-PNF-DZC7	Moonlight	0.90	812,002	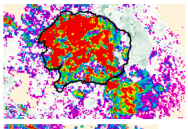
2002-CO-PSF-404	Hayman	0.85	702,088	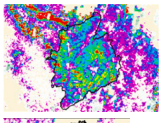
2011-NM-N6S-F5PS	Las Conchas[2]	0.70	662,816	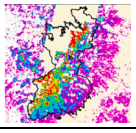

Notes: 1. 2001 forest fraction was determined with respect to the National Land Cover Database (NLCD) 2016 product (Dewitz, 2019). 2. Some data for the NW part of this fire were missing.

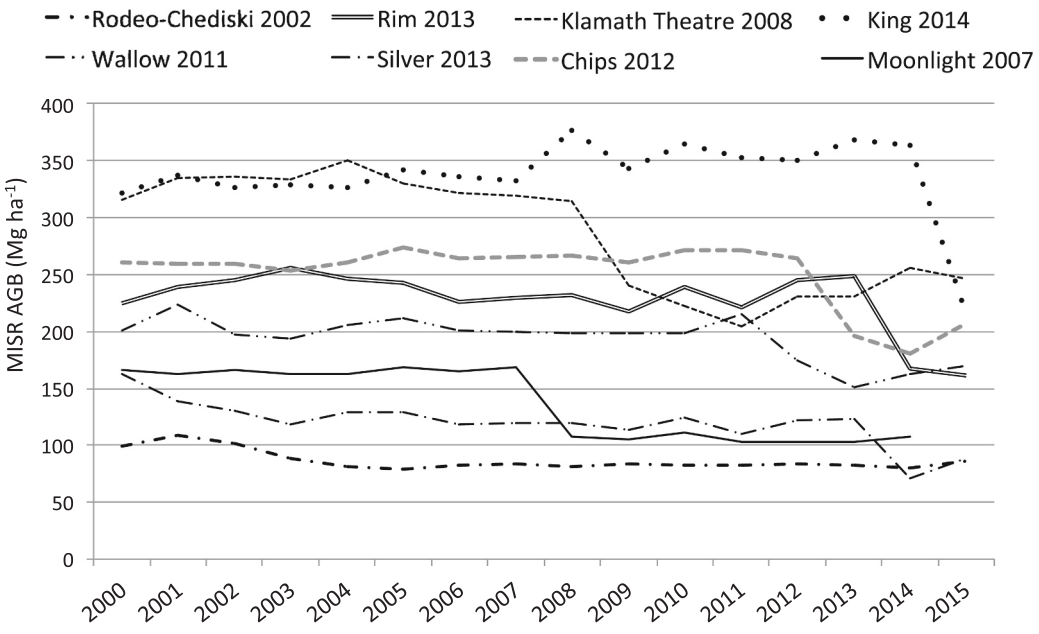

Fig. 16. AGB trajectories for selected locations within large forest fires. Locations: Rodeo-Chediski 110:37:29.55 W 34:18:24.87 N; Rim 120:00:33.78 W 37:59:13.57 N; Klamath Theatre 123:47:49.75 W 41:34:12.63 N; King 120:34:05.65 W 38:50:15.92 N; Wallow 109:20:36.49 W 33:40:21.21 N; Silver 107:46:19.16 W 32:52:50.28 N; Chips 121:10:21.14 W 40:05:54.92 N; and Moonlight 120:44:06.63 W 40:16:02.25 N.

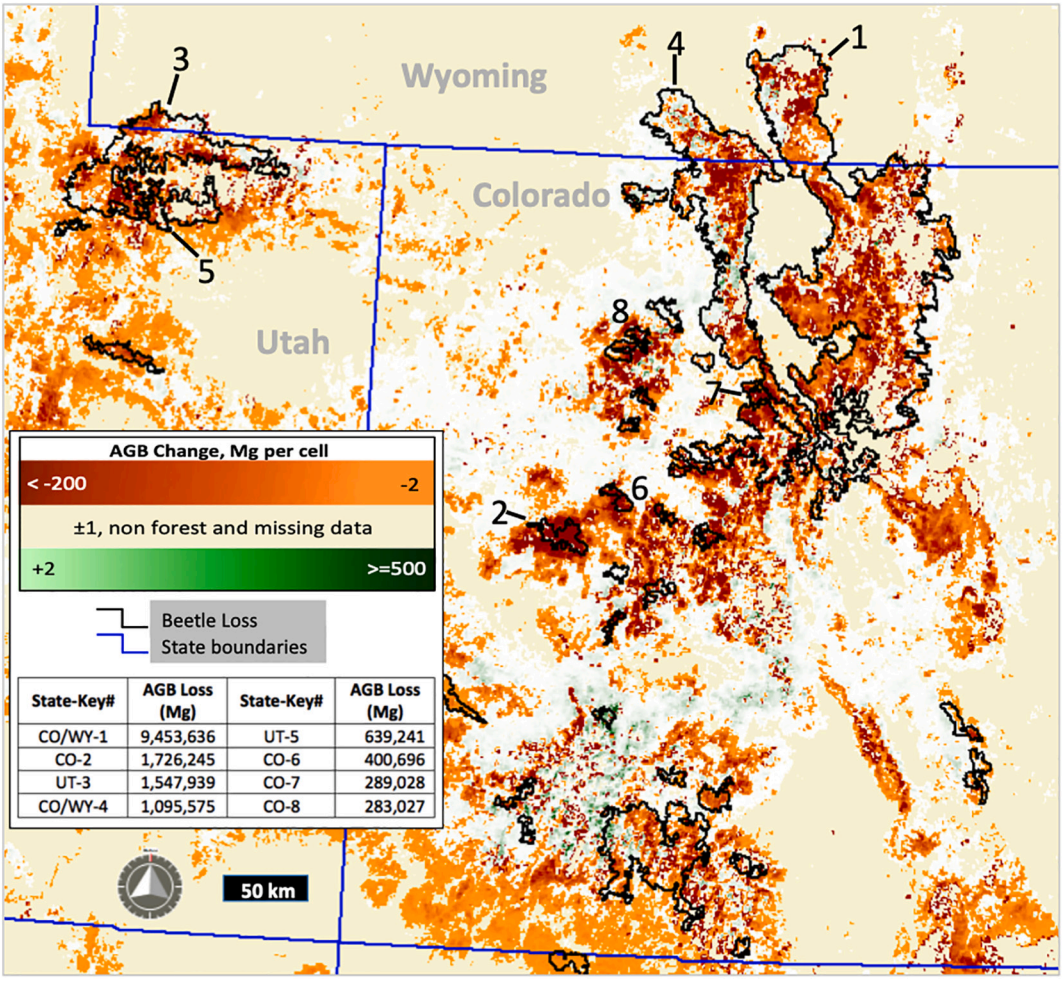

State-Key#	AGB Loss (Mg)	State-Key#	AGB Loss (Mg)
CO/WY-1	9,453,636	UT-5	639,241
CO-2	1,726,245	CO-6	400,696
UT-3	1,547,939	CO-7	289,028
CO/WY-4	1,095,575	CO-8	283,027

Fig. 17. Change in MISR-derived AGB over the period (2014/15 composite minus 2000/2001 composite) for pine beetle loss areas for 2003 to 2012. Areas from Berner et al. (2017a), filtered to include only those larger than 50 km^2 (12,355 acres).

4. Conclusions

This study has demonstrated the application of multi-angle 672 nm (red) band reflectance data for mapping forest aboveground biomass over large areas – the entire southwestern United States – and inter-annually from 2000 to 2015. It shows that it is possible to leverage the surface structural information captured in the multi-angle reflectance data in an approach that does not require reflectance model inversion depending on estimation of the under-canopy background BRDF for each location a priori, which can be challenging and difficult to validate. The main conclusions from this study are:

1. A multi-angle index derived from MISR red band BRFs modeled at MISR view zenith angles in the SPP predicted forest AGB with reasonably good precision with respect to NBCD 2000 radar-based, CMS GLAS-derived, and CMS airborne lidar-derived AGB estimates (R^2 of 0.75 and 0.66 and RMSE of 59.2 and 82.8 for the last two, respectively, with respect to the MISR AGB for the Rim Fire area).
2. The 2005 MISR MAI-derived forest AGB map for the entire southwestern United States was spatially consistent with the 2005 ICESat GLAS AGB map trained with FIA data map ($N = 11{,}019{,}944$ 250 m^2 locations, excluding missing and invalid data), yielding an R^2 of 0.90 and an RMSE of 37 Mg ha^{-1}.
3. Forest AGB trajectories from the MISR multi-angle index were more stable through time than those predicted using BRFs or BRDF model kernel weights and tracked the CMS 2005 and 2013 lidar-derived estimates well.
4. This method does not have sufficient sensitivity to vegetation structure to allow the mapping of woody plants of short stature (i.e., shrubs). There is reduced sensitivity compared to canopy reflectance model inversion (an approach that has its own limitations: too many unknowns), or the leveraging of BRDF model kernel weights plus nadir-spectral BRFs (e.g., Duchesne et al., 2018).
5. MISR-derived forest biomass loss corresponds well with published wildfire and beetle perimeters. The forest AGB net change map also shows areas that may be affected by forest harvest, thinning, or drought.

The forest AGB maps derived here using this multi-angle index approach are being made available at the Oak Ridge National Laboratory (ORNL) Distributed Active Archive Center (DAAC) at doi:https://doi.org/10.3334/ORNLDAAC/1978, together with metadata documentation and quality assurance layers: flags for all estimates that indicate missing NBCD 2000 or year 2000 MISR data, and for all subsequent years and locations: BRDF model fitting >0.008 that indicates snow as well as cloud cover, estimates greater than the NBCD 2000 estimate +100, and missing MISR data, e.g., locations where there were too few BRFs to invert the BRDF model. These raster maps are preliminary, research-level outputs and not intended as polished, final products, as there are some gaps and anomalies from missing data, as well as compositing artefacts. Further evaluations of the maps generated by this study as well as those for other regions can leverage other CMS lidar-based AGB data sets, as well as forest canopy analysis using high resolution imagery + allometry – e.g., from CANAPI (Chopping, 2011; Chopping et al., 2014; Duchesne et al., 2015) – and AGB estimates derived from GEDI waveforms in the L4A and L4B products that cover larger areas with greater consistency and precision (Dubayah et al., 2020).

Using NBCD 2000 or CMS GLAS estimates to retrieve maps of model coefficients across the conterminous U.S. could enable generation of MISR-derived forest AGB map series for all years from 2000 on. MISR data simulated using the Rahman-Pinty-Verstraete (RPV) model (Rahman et al., 1993) – whose coefficients are readily available at 1.1 km spatial resolution as part of the MISR Level 2 Land Surface Product (MIL2ASLS_3) – could also be utilized. Although the MISR MAI approach predicts forest AGB quite well for a region that is characterized by bright soils and sparse understories, a more flexible approach may be required for broader areas with different soils, forest canopies, and vegetation associations (e.g., modern machine learning approaches such as Keras/TensorFlow deep neural networks; further research is required to determine the relative merits of different approaches.

The MISR-developed MAI approach might also be explored using other BRDF data and over other regions, perhaps using other BRDF models (e.g., RPV, Roujean (Roujean et al., 1992), or Walthall (Walthall et al., 1985), or the RossThickLiSparse-Reciprocal (Schaaf et al., 2002). Although the lifetime of the MISR instrument is necessarily limited to December 2025 by the lack of fuel required to sustain the Terra satellite in orbit, its record already provides a two-decade record; furthermore, NASA and other multi-angle imagers are in the planning stages (e.g., MAIA, HARP2 and SPEXone on PACE). The significance of this work potentially goes beyond this region and the particular sensor used: since the multi-angle index is obtained using a modeled red band BRF dataset, any BRDF dataset or product could be used to generate it, e.g., BRDF products from MODIS (on Terra and Aqua), VIIRS (on board Suomi NPP launched in 2011, NOAA-20 launched in 2017, and JPSS-2, scheduled to be launched in 2022), or Sentinel-3A and —3B (launched in 2016 and 2018, respectively; León-Tavares et al., 2020).

CRediT authorship contribution statement

Mark Chopping: Conceptualization, Methodology, Investigation, Data curation, Writing – original draft, Writing – review & editing, Funding acquisition. **Zhuosen Wang:** Software, Writing – review & editing. **Crystal Schaaf:** Writing – original draft, Writing – review & editing. **Michael A. Bull:** Software, Resources, Writing – original draft. **Rocio R. Duchesne:** Writing – review & editing.

Declaration of Competing Interest

The authors declare that they have no known competing financial interests or personal relationships that could have appeared to influence the work reported in this paper.

Acknowledgements

This research was supported by NASA JPL subcontracts #1365499 and #1552327 to MC. Some of the initial data processing was performed as part of NASA project #NNX11AF90G: The Science of Terra and Aqua, "A Decade of Changes in Aboveground Live Standing Dry Biomass, Canopy Cover, Height, and Understory Density in the Southwestern United States from EOS MISR and MODIS", 3/3/2011 - 12/31/2016. Thanks to Xiaohong Chopping for informed comments and suggestions, to Sassan Saatchi (NASA JPL) for advice on the CMS GLAS data set and Jonathan Greenberg for advice on the CMS aerial lidar-based data set. We also acknowledge the work of the three peer reviewers, whose insights resulted in tangible improvements to the manuscript. The MISR data products used were obtained using the MISR Order and Customization Tool hosted at the NASA Langley Atmospheric Science Data Center (http://l0dup05.larc.nasa.gov/MISR/cgi-bin/MISR/main.cgi) and accessible via NASA Earthdata (https://earthdata.nasa.gov/), except as otherwise noted; updated LAND data sets were provided by co-author Michael Bull. The NASA Carbon Monitoring System was responsible for funding the airborne lidar surveys and development of the ICESat-based data sets used here. The NBCD 2000 data set was from Kellndorfer et al. (2013); additional citation: Kellndorfer, J., Walker, W., Kirsch, K., Fiske, G., Bishop, J., LaPoint, L., Hoppus, M., and Westfall, J.

(2007-2009). The National Biomass and Carbon Dataset 2000 (NBCD 2000). The Woods Hole Research Center, Falmouth, MA.

Appendix A

Table A1
Sites selected in the Mt. Lindsey, Colorado study area.

Site	Latitude (DMS)	Longitude W (DMS)	MISR MAI (DA/AA)/CF	AGB, Mg ha^{-1} NBCD 2000	Forest NDVI	Forest WoD* for NBAR45
Forest 1	37 38 26	105 27 17.1	80.9	186	0.59	1.7
Forest 7	37 38 16	105 27 14.0	75.3	173	0.56	1.9
Forest 2	37 38 56	105 21 10.1	58.8	146	0.67	1.9
Forest 5, on Rock	37 35 58	105 28 22.7	13.6	145	0.39	1.9
Forest 3	37 33 43	105 26 35.5	44.4	141	0.59	2.8
Forest 6	37 32 13	105 23 54.8	17.6	50	0.49	1.9
Forest 4	37 31 18	105 30 55.5	14.8	33	0.36	1.9
Forest 8	37 38 16	105 16 58.5	40.2	143	0.64	1.9
Forest 9	37 35 15	105 23 34.9	36.2	101	0.69	1.9
Forest10	37 38 47	105 29 42.0	45.3	138	0.53	1.9
Forest11	37 39 1	105 22 7.49	75.0	160	0.71	4.0
Forest12	37 29 55	105 13 58.9	28.8	89	0.61	3.3
Forest13	37 23 59	105 13 11.0	57.7	149	0.64	4.1
Forest14	37 25 28	105 13 58.0	29.7	57	0.59	1.9
Forest15	37 24 17	105 17 8.33	39.4	116	0.60	1.9
Forest16	37 30 32	105 15 34.3	22.3	40	0.47	1.9
Forest17	37 20 38	105 17 26.6	29.5	106	0.54	3.3
Forest18	37 22 56	105 23 35.3	14.2	21	0.34	3.2
Forest19	37 34 17	105 33 0.26	24.6	99	0.50	1.9
Forest20	37 39 24	105 15 23.5	49.0	135	0.63	1.9
Forest21, on Rock	37 37 13	105 28 9.85	13.9	118	0.43	1.9
Crop Circle 1	37 23 36	105 25 43.3	24.4	N/A	N/A	N/A
Crop Circle 2	37 23 10	105 25 31.1	34.7	N/A	N/A	N/A
Crop Circle 3	37 25 28	105 29 10.4	16.9	N/A	N/A	N/A
Lake	37 23 42	105 23 11.6	66.4	N/A	N/A	N/A
Desert 1	37 27 40	105 23 4.10	10.1	N/A	N/A	N/A
Desert 2	37 28 35	105 23 0.30	8.1	N/A	N/A	N/A
N.Stream	37 30 3	105 23 47.3	15.0	N/A	N/A	N/A
S.Stream	37 27 35	105 25 23.4	11.5	N/A	N/A	N/A
Snow_bright	37 34 59	105 28 54.7	3.5	N/A	N/A	N/A

Note: * WoD = Weight of Determination, a noise amplification factor, see Lucht and Lewis, 2000. NBAR is Normalized, BRDF-Adjusted Reflectance, see Schaaf et al., 2002.

References

Abatzoglou, J.T., Williams, A.P., 2016. Climate change has added to western US forest fire. Proc. Natl. Acad. Sci. 113 (42), 11770–11775. https://doi.org/10.1073/pnas.1607171113.

Bergen, K.M., Goetz, S.J., Dubayah, R.O., Henebry, G.M., Hunsaker, C.T., Imhoff, M.L., Nelson, R.F., Parker, G.G., Radeloff, V.C., 2009. Remote sensing of vegetation 3−D structure for biodiversity and habitat: review and implications for lidar and radar spaceborne missions. J. Geophys. Res. 114, G00E06. https://doi.org/10.1029/2008JG000883.

Berner, L.T., Law, B.E., Meddens, A.J., Hicke, J.A., 2017a. Tree Mortality from Fires and Bark Beetles at 1-km Resolution, Western USA, 2003-2012. ORNL DAAC, Oak Ridge, Tennessee, USA. https://doi.org/10.3334/ORNLDAAC/1512.

Berner, L.T., Law, B.E., Meddens, A.J.H., Hicke, J.A., 2017b. Tree mortality from fires, bark beetles, and timber harvest during a hot and dry decade in the western United States (2003−2012). Environ. Res. Lett. 12 (6) https://doi.org/10.1088/1748-9326/aa6f94.

Blackard, J.A., Finco, M.V., Helmer, E.H., Holden, G.R., Hoppus, M.L., Jacobs, D.M., Lister, A.J., Moisen, G.G., Nelson, M.D., Riemann, R., Ruefenacht, B., Salajanu, D., Weyermann, D.L., Winterberger, K.C., Brandeis, T.J., Czaplewski, R.L., McRoberts, R.E., Patterson, P.L., Tymcio, R.P., 2008. Mapping U.S. forest biomass using nationwide forest inventory data and moderate resolution information. Remote Sens. Environ. 112, 1658–1677.

Breidenbach, J., Koch, B., Kändler, G., Kleusberg, A., 2008. Quantifying the influence of slope, aspect, crown shape and stem density on the estimation of tree height at plot level using lidar and InSAR data. Int. J. Remote Sens. 29 (5), 1511–1536.

Brent, R.P., 1973. Algorithms for Minimization without Derivatives. Prentice Hall, Englewood Cliffs, NJ. Reprinted by Dover Publications, Mineola, New York, 2002; 2013.

Burkardt, J., 2019. Brent Algorithm Code Distribution Page "BRENT: Algorithms for Minimization Without Derivatives" under the John Burkardt homepage at the University of South Carolina, at. https://people.math.sc.edu/Burkardt/c_src/brent/brent.html. Last revised on 22 January 2019; last access January 10, 2022.

Chen, J.M., Lui, J., Leblanc, S.G., Lacaze, R., Roujean, J-L., 2003. Multi-angular optical remote sensing for assessing vegetation structure and carbon absorption. Remote. Sens. Environ. 84 (4), 516–525. https://doi.org/10.1016/S0034-4257(02)00150-5.

Chopping, M.J., 2001. Testing LiSK BRDF models over a semiarid grassland region with visible and near-infrared ATSR-2 and AVHRR data. Int. J. Remote Sens. 22, 3533–3552.

Chopping, M., 2011. CANAPI: canopy analysis with panchromatic imagery. Remote Sens. Lett. 2 (1), 21–29 published 17 June 2010. https://doi.org/10.1080/01431161.2010.486805.

Chopping, M., North, M., Chen, J., Schaaf, C.B., Blair, J.B., Martonchik, J.V., Bull, M., 2012. Forest cover and height from MISR in a topographically complex landscape assessed with high quality reference data. IEEE Journal of Selected Topics in Applied Earth Observations and Remote Sensing (JSTARS) 5 (1), 44–58.

Chopping, M., Duchesne, R., North, M., 2014. Assessing remotely-sensed aboveground biomass estimates in the Sierra National Forest. In: Proc. 2014 IEEE International Geoscience and Remote Sensing Symposium (IGARSS'14), Quebec City, Canada, July 13-18, 2014, pp. 1041–1044.

Chopping, M., Wang, Z., Schaaf, C., Duchesne, R., 2015. Changes in Aboveground Biomass in the Southwestern United States 2000–2009 from MISR, 5th North American Carbon Progam all-Investigators' Meeting, Jan. 26–29, 2015, Washington, DC. available at. https://nacarbon.org/meeting_ab_presentations/2015/2015_Poster_Chopping_89_335.pdf.

Chopping, M., Bull, M., Wang, Z., Duchesne, R., 2018. Changes in Forests of the Southwestern United States from MISR, 2000–2015, NASA MISR Science Team Meeting, California Institute of Technology, Pasadena, CA, February 14-15, 2018.

Chopping, M., Bull, M., Wang, Z., Duchesne, R., 2019. Mapping Forests of the Southwestern United States using MISR. In: 2019 MISR Science Team Meeting, Pasadena, CA, February 12–13, 2019.

Clark, M.L., Clark, D.B., Roberts, D.A., 2004. Small-footprint lidar estimation of sub-canopy elevation and tree height in a tropical rain forest landscape. Remote Sens. Environ. 91 (1), 68–89. https://doi.org/10.1016/j.rse.2004.02.008.

Dennison, P.E., Brewer, S.C., Arnold, J.D., Moritz, M.A., 2014. Large wildfire trends in the western United States, 1984–2011. Geophys. Res. Lett. 41, 2928–2933. https://doi.org/10.1002/2014GL059576.

Dewitz, J., 2019. National Land Cover Database (NLCD) 2016 Products: U.S. Geological Survey Data Release. https://doi.org/10.5066/P96HHBIE.

Diner, D.J., Asner, G.P., Davies, R., Knyazikhin, Y., Muller, J.-P., Nolin, A.W., Pinty, B., Schaaf, C.B., Stroeve, J., 1999. New directions in earth observing: scientific applications of multi-angle remote sensing. Bull. Am. Meteorol. Soc. 80 (11), 2209–2229.

Diner, D.J., Braswell, B.H., Davies, R., Gobron, N., Hu, J., Jin, Y., Kahn, R.A., Knyazikhin, Y., Loeb, N., Muller, J.-P., Nolin, A.W., Pinty, B., Schaaf, C.B., Seiz, G., Stroeve, J., 2005. The value of multiangle measurements for retrieving structurally and radiatively consistent properties of clouds, aerosols, and surfaces. Remote Sens. Environ. 97, 495–518.

Dubayah, R., Blair, J.B., Goetz, S., Fatoyinbo, L., Hansen, M., Healey, S., Hofton, M., Hurtt, G., Kellner, J., Luthcke, S., Armston, J., 2020. The global ecosystem dynamics investigation: high-resolution laser ranging of the earth's forests and topography. Sci. Remote Sens. 100002.

Dubayah, R.O., Armston, J., Kellner, J.R., Duncanson, L., Healey, S.P., Patterson, P.L., Hancock, S., Tang, H., Bruening, J., Hofton, M.A., Blair, J.B., Luthcke, S.B., 2021. GEDI L4A Footprint Level Aboveground Biomass Density, Version 2. ORNL DAAC, Oak Ridge, Tennessee, USA. https://doi.org/10.3334/ORNLDAAC/1986.

Duchesne, R.R., Chopping, M.J., Tape, K.D., 2015. Capability of the CANAPI algorithm to derive shrub structural parameters from satellite imagery in the Alaskan Arctic. Polar Rec. https://doi.org/10.1017/S0032247415000509 available on CJO2015.

Duchesne, R.R., Chopping, M.J., Tape, K.D., Wang, Z., Schaaf, C., 2018. Changes in tall shrub abundance on the North Slope of Alaska, 2000–2010. Remote Sens. Environ. 219, 221–232.

Duncanson, L., Armston, J., Disney, M., et al., 2019. The importance of consistent global forest aboveground biomass product validation. Surv. Geophys. 40, 979–999. https://doi.org/10.1007/s10712-019-09538-8.

Hagen, S., Harris, N., Saatchi, S.S., Pearson, T., Woodall, C.W., Ganguly, S., Domke, G.M., Braswell, B.H., Walters, B.F., Jenkins, J.C., Brown, S., Salas, W.A., Fore, A., Yu, Y., Nemani, R.R., Ipsan, C., Brown, K.R., 2016. CMS: Forest Carbon Stocks, Emissions, and Net Flux for the Conterminous US: 2005-2010. ORNL DAAC, Oak Ridge, Tennessee, USA. https://doi.org/10.3334/ORNLDAAC/1313.

Harris, N.L., Hagen, S.C., Saatchi, S.S., Pearson, T.R.H., Woodall, C.W., Domke, G.M., Braswell, B.H., Walters, B.F., Brown, S., Salas, W., Fore, A., Yu, Y., 2016. Attribution of net carbon change by disturbance type across forest lands of the conterminous United States. Carb. Bal. Manag. 11 (1), 24. https://doi.org/10.1186/s13021-016-0066-5, 2016 Nov 14.

Heiskanen, J., 2006. Tree cover and height estimation in the Fennoscandian tundrataiga transition zone using multiangular MISR data. Remote Sens. Environ. 103, 97–114.

Herold, M., Carter, S., Avitabile, V., et al., 2019. The role and need for space-based forest biomass-related measurements in environmental management and policy. Surv. Geophys. 40, 757–778. https://doi.org/10.1007/s10712-019-09510-6.

Interoffice Memorandum MISR SDS DFM-0827-F, August 12, 2016, To: Design File, From: Mike Bull, "Aerosol Optical Depth Smoothing Algorithm", 2016. Jet Propulsion Laboratory.

Jet Propulsion Laboratory, 2020a. MISR Toolkit Pages. at github at. https://nasa.github.io/MISR-Toolkit/html/index.html. last access 1/15/21.

Jet Propulsion Laboratory, 2020b. Introducing the New MISR Aerosol Product, 02.10.2020. Online news article with animation at. https://misr.jpl.nasa.gov/news/news/index.cfm?FuseAction=ShowNews&NewsID=166. last access 1/25/21.

Kellndorfer, J., Walker, W., Kirsch, K., Fiske, G., Bishop, J., LaPoint, L., Hoppus, M., Westfall, J., . NACP Aboveground Biomass and Carbon Baseline Data, V. 2 (NBCD 2000), U.S.A., 2000. Data set. Available on-line. http://daac.ornl.gov. from. ORNL DAAC, Oak Ridge, Tennessee, USA. https://doi.org/10.3334/ORNLDAAC/1161.

Lefsky, M.A., Harding, D.J., Keller, M., Cohen, W.B., Carabajal, C.C., Espirito-Santo, F.D. B., Hunter, M.O., de Oliveira Jr, R., 2005. Estimates of forest canopy height and aboveground biomass using ICESat. Geophys. Res. Lett. 32, L22S02. https://doi.org/10.1029/2005GL023971.

León-Tavares, J., et al., 2020. Copernicus Global Land Operations Vegetation and Energy/CGLOPS-1: Framework Service Contract N° 199494 (JRC) Algorithm Theoretical Basis Document BRDF Model Retrieval from Sentinel-3 Collection 300m. v1. June 19, 2020. https://land.copernicus.eu/global/sites/cgls.vito.be/files/products/CGLOPS1_ATBD_BRDFCorrection300m-V1_I1.00.pdf. Last access January 10, 2022.

Li, X., Strahler, A.H., 1985. Geometric-optical modeling of a conifer forest canopy. IEEE Trans. Geosci. Remote Sens. 23, 705–721.

Lucht, W., Lewis, P., 2000. Theoretical noise sensitivity of BRDF and albedo retrieval from the EOS-MODIS and MISR sensors with respect to angular sampling. Int. J. Remote Sens. 21, 81–98.

Narine, L.L., Popescu, S., Malambo, L., 2020. Using ICESat-2 to estimate and map forest aboveground biomass: a first example. Remote Sens. 12 (11), 1824. https://doi.org/10.3390/rs12111824.

Qiu, F., Zhang, Q., 2020. Multi-angular observation of forest canopy reflectance based on a hyperspectral UAV imaging platform. In: EGU General Assembly 2020, Online, 4–8 May 2020, EGU2020-18629. https://doi.org/10.5194/egusphere-egu2020-18629, 2020. Last access: March 13. 2020.

Rahman, H., Pinty, B., Verstraete, M.M., 1993. Coupled surface-atmosphere reflectance (CSAR) model, 2, Semiempirical surface model usable with NOAA advanced very high resolution radiometer data. J. Geophys. Res. Atmos. 1993 (98), 20791–20801.

Roujean, J-L., Leroy, M., Deschamps, P-Y., 1992. A bidirectional reflectance model of the Earth's surface for the correction of remote sensing data. J. Geophys. Res. Atmos. 97 (D18), 20455–20468. https://doi.org/10.1029/92JD01411.

Saatchi, S.S., Harris, N.L., Brown, S., Lefsky, M., Mitchard, E.T.A., Salas, W., Zutta, B.R., Buermann, W., Lewis, S.L., Hagen, S., Petrova, S., White, L., Silman, M., Morel, A., 2011. Benchmark map of forest carbon stocks in tropical regions across three continents. Proc. Natl. Acad. Sci. 108 (24), 9899–9904. https://doi.org/10.1073/pnas.1019576108. Jun 2011.

Schaaf, C., Gao, F., Strahler, A., Lucht, W., Li, X., Tsang, T., Strugnell, N., Zhang, X., Jin, Y., Muller, J.-P., Lewis, P., Barnsley, M., Hobson, P., Disney, M., Roberts, G., Dunderdale, M., Doll, C., d'Entremont, R., Hu, B., Roy, D., 2002. First operational BRDF, albedo nadir reflectance products from MODIS. Remote Sens. Environ. 83, 135–148. https://doi.org/10.1016/S0034-4257(02)00091-3.

Schull, M.A., et al., 2007. Physical interpretation of the correlation between multi−angle spectral data and canopy height. Geophys. Res. Lett. 34, L18405. https://doi.org/10.1029/2007GL031143.

Strahler, A.H., Wanner, W., Schaaf, C., Li, X., Hu, B., Muller, J.-P., Lewis, P., Barnsley, M., 1996. MODIS BRDF/Albedo Product: Algorithm Theoretical Basis Documentation. Version 4.0, NASA/EOS ATBD, 94 pp.

Walters, S.P., Schneider, N.J., Guthrie, J.D., 2011. Geospatial Multi-Agency Coordination (GeoMAC) Wildland Fire Perimeters, 2008: U.S. Geological Survey Data Series 612, 6 p.

Walthall, C.L., Norman, J.M., Welles, et al., 1985. Simple equation to approximate the bidirectional reflectance from vegetative canopies and bare surfaces. Appl. Opt. 24, 383–387.

Wang, Z., Schaaf, C.B., Lewis, P., Knyazikhin, Y., Schull, M.A., Strahler, A.H., Yao, T., Myneni, R.B., Chopping, M., 2011. Retrieval of canopy vertical structure using MODIS data. Remote Sens. Environ. 115 (6), 1595–1601.

Wang, Q., Pang, Y., Li, Z., Sun, G., Chen, E., Ni-Meister, W., 2016. The potential of forest biomass inversion based on vegetation indices using multi-angle CHRIS/PROBA data. Remote Sens. 8 (11), 891. https://doi.org/10.3390/rs8110891.

Wanner, W., Li, X., Strahler, A.H., 1995. On the derivation of kernels for kernel-driven models of bidirectional reflectance. J. Geophys. Res. 100, 21077–21090.

Westerling, A.L., 2016. Increasing western US forest wildfire activity: sensitivity to changes in the timing of spring. Philos. Trans. R. Soc. Lond. Ser. B Biol. Sci. 371 (1696), 20150178. https://doi.org/10.1098/rstb.2015.0178.

Williams, A.P., Abatzoglou, J.T., Gershunov, A., Guzman-Morales, J., Bishop, D.A., Balch, J.K., Lettenmaier, D.P., 2019. Observed impacts of anthropogenic climate change on wildfire in California. Earth's Future 7, 892–910. https://doi.org/10.1029/2019EF001210.

Xiao, J., Chevallier, F., Gomez, C., Guanter, L., Hicke, J.A., Huete, A.R., Ichii, K., Ni, W., Pang, Y., Rahman, A.F., Sun, G., Yuan, W., Zhang, L., Zhang, X., 2019. Remote sensing of the terrestrial carbon cycle: a review of advances over 50 years. Remote Sens. Environ. 233, 111383. https://doi.org/10.1016/j.rse.2019.111383.

Xu, Q., Man, A., Fredrickson, M.M., Hou, Z., Pitkanen, J., Wing, B., Ramirez, C., Li, B., Greenberg, J., 2018a. LiDAR-Derived Aboveground Biomass and Uncertainty for California Forests, 2005–2014. ORNL DAAC, Oak Ridge, Tennessee, USA.

Xu, Q., Man, A., Fredrickson, M., Hou, Z., Pitkänen, J., Wing, B., Ramirez, C., Li, B., Greenberg, A.J., 2018b. Quantification of uncertainty in aboveground biomass estimates derived from small-footprint airborne LiDAR. Remote Sens. Environ. 216, 514–528. https://doi.org/10.1016/j.rse.2018.07.022.

Zhang, G., Ganguly, S., Nemani, R.R., White, M.A., Milesi, C., Hashimoto, H., Wang, W., Saatchi, S., Yu, Y., Myneni, R.B., 2014. Estimation of forest aboveground biomass in California using canopy height and leaf area index estimated from satellite data. Remote Sens. Environ. 151, 44–56.